

# The direct synthesis of dimethyl carbonate out of carbon dioxide and methanol is catalyzed by D-metals supported on various matrices

Douglas José Faria<sup>a</sup>, Leonardo Moreira dos Santos<sup>b</sup>, Franciele Longaray Bernard<sup>b</sup>, Ingrid Selbacch Pinto<sup>b</sup>, Vitaly V. Chaban<sup>c</sup>, Ivan Pacheco Romero<sup>d</sup>, Sandra Einloft<sup>a,b,\*</sup>

<sup>a</sup> Post-Graduation Program in Materials Engineering and Technology, Pontifical Catholic University of Rio Grande do Sul – PUCRS, Porto Alegre, Brazil

<sup>b</sup> School of Technology, Pontifical Catholic University of Rio Grande do Sul PUCRS, Porto Alegre, Brazil

<sup>c</sup> Yerevan State University, Yerevan, Armenia

<sup>d</sup> CENPES/Petrobras, Rio de Janeiro, Brazil

## ARTICLE INFO

### Keywords:

Dimethyl carbonate  
CO<sub>2</sub>  
Methanol  
Catalysts  
Synthesis

## ABSTRACT

The chemical transformation of carbon dioxide (CO<sub>2</sub>) into valuable chemicals is a fascinating way to reduce CO<sub>2</sub> concentration in the atmosphere. Dimethyl carbonate (DMC) exhibits low toxicity, biodegradability, and versatile reactivity. DMC production by direct synthesis using CO<sub>2</sub> and methanol (CH<sub>3</sub>OH) may be one of the ever most promising green routes. On the other hand, direct synthesis of DMC shows some drawbacks including unfavorable thermochemistry and quick deactivation of catalysts. The development of new catalytic systems currently represents an urgent agenda to overcome these disadvantages. This study investigates the catalytic activity of iron (Fe) and copper (Cu) catalysts supported on alumina (AL), silica (SI), and eggshells (ES) during the course of DMC production by direct synthesis. The supported catalysts were synthesized using the impregnation method and characterized by TGA, BET, DTP-NH<sub>3</sub>, XRD, and FESEM/EDS. The contents of the impregnated iron in the matrices are ES-Fe (13%) > AL-Fe (6%) > SI-Fe (4%). The contents of the impregnated copper are ES-Cu (7%) > AL-Cu (3%) = SI-Cu (3%). The DMC conversions equal 8.9 (AL-Cu), 6.2 (SI-Cu), 11.3% (ES-Cu), 6.1 (AL-Fe), 7.2 (SI-Fe), and 12.7% (ES-Fe). The ES-Fe recycle demonstrated stability of the catalytic action in the first and second reuse, maintaining high conversion and selectivity of DMC. All tests reveal a DMC selectivity of over 99%. The reported results suggest that the catalytic DMC production depends both on the nature of d-metal and support, whereas the ES-Fe system exhibits the best performance.

## 1. Introduction

The use of captured carbon dioxide (CO<sub>2</sub>) as a raw material in the chemical industries represents a great value when considering the environmental benefits. However, due to the large amount of energy required for its transformation, industrial processes using CO<sub>2</sub> as a starting material are still scarce [28]. Substantial research and development efforts are being carried out to use CO<sub>2</sub> to produce chemicals contributing to CO<sub>2</sub> emissions reduction [60,80,91].

Focusing on CO<sub>2</sub> emissions mitigation, the development of innovative CO<sub>2</sub> separation, sequestration, and utilization processes is vital [20, 35]. For CO<sub>2</sub> transformation reactions, catalyst choice, temperature, and pressure are very important for reaction optimization allowing sustainable production of different organic compounds [75].

Among the organic compounds that can be produced from the CO<sub>2</sub> chemical transformation, carbonates are worth mentioning. These molecules can selectively and efficiently replace hazardous reagents in some organic processes [14,78,89]. Organic carbonates can be divided into two groups: linear carbonates: dimethyl carbonate (DMC) and diethyl carbonate (DEC); and cyclic carbonates: ethylene carbonate (CE), propylene carbonate (CP), butylene carbonate (CB), and glycerol carbonate (GC) [13,53,54,71,76].

DMC, methanol, and methane were named the most interesting products from CO<sub>2</sub> transformation [58]. DMC is an important chemical intermediate of easy degradability, high polarity, low viscosity, and toxicity, used in a wide range of applications [11,26,64,76]. DMC is used as an intermediate in polycarbonate synthesis, a widely used polymer in the construction, automobile, and medical device industries, as an

\* Corresponding author at: Post-Graduation Program in Materials Engineering and Technology, Pontifical Catholic University of Rio Grande do Sul – PUCRS, Porto Alegre, Brazil.

E-mail address: [einloft@pucrs.br](mailto:einloft@pucrs.br) (S. Einloft).

<https://doi.org/10.1016/j.molstruc.2023.136110>

Received 1 May 2023; Received in revised form 14 June 2023; Accepted 27 June 2023

Available online 28 June 2023

0022-2860/© 2023 Elsevier B.V. All rights reserved.

electrolyte solvent for lithium batteries due to its high dielectric constant, and environmentally friendly reagent for methylation and carbonylation [17,26].

Several routes have been proposed to synthesize DMC, such as the phosgene route, transesterification, urea alcoholysis, methanol oxidative carbonylation, and – naturally – the direct synthesis route from methanol and CO<sub>2</sub> [21,64]. Among these routes, phosgenation, methanol oxidative carbonylation (oxy-carbonylation) in a liquid phase, and transesterification reached the stage of industrialization. However, the phosgenation route was discontinued due to the raw material's (phosgene) high toxicity. In turn, the oxy-carbonylation and transesterification routes continue to be intensively used in DMC industrial production, although they have some disadvantages, such as reagents' high toxicity and corrosion [21,90].

To overcome these disadvantages, DMC direct synthesis is being widely studied to improve DMC yield using nontoxic non-corrosive reagents [5,11,13,31,33,46,53,73,83]. Fig. 1 presents the chemical route of the DMC direct synthesis.

The production of DMC through direct synthesis offers a straightforward and eco-friendly approach, utilizing a minimal number of reagents. CO<sub>2</sub>, a key component with environmental concerns, serves as one of the primary starting materials. However, the application of this method is hindered by the equilibrium dynamics of the reaction. Under mild temperatures and pressures, the spontaneous formation of DMC is impeded as it possesses positive Gibbs energy, resulting in low yields. Consequently, more intricate conditions involving higher pressures and temperatures are necessary, adding complexity to the process. One of the significant obstacles involves the generation of water during synthesis, causing a shift in the reaction equilibrium towards the reactants and diminishing the conversion of methanol into DMC. Hence, to overcome this challenge, optimizing parameters such as temperature, pressure, dehydrating agents, and selective and reusable heterogeneous catalysts emerge as viable alternatives [81].

Several homogeneous catalysts were used in DMC production by direct synthesis, thallium (I) hydroxide, tin (IV), tetraalkoxides, dialkyltin dialkoxides, bases, C, N-chelated organotin (IV) trifluoromethane sulfonates and titanium (IV) tetraalkoxides [19,27,34,43,72,84,92,94]. However, catalyst separation from the reaction medium is difficult when using homogeneous catalysts. The use of heterogeneous catalysts, such as CeO<sub>2</sub>, ZrO<sub>2</sub> [48,74], Ce<sub>0.5</sub>Zr<sub>0.5</sub>O<sub>2</sub> [100], Ce<sub>0.4</sub>Zr<sub>0.6</sub>O<sub>2</sub> [46], and Cu-CeO<sub>2</sub> [88], can overcome this problem by facilitating the catalyst separation from products.

In addition to the use of conventional catalysts, metals supported in different solids, such as silica, activated carbon, alumina, and food waste as eggshells, appear as a good choice presenting comparable activity with homogeneous catalysts and the easy separation of heterogeneous ones [1,23,32,37,39,42,87]. The eggshell presents high thermal stability, low density, and a highly porous structure similar to activated carbon, providing a higher specific surface area. The eggshell is around 10% of the egg corresponding to around 5.92 million tons of this waste per year worldwide [16]. The composition of eggshells is approximately 98% Ca and 2% Mg/Fe/Nit

Solid supports impregnated with metals can be active catalysts in the DMC direct synthesis increasing product yield and selectivity. Yet, a heterogeneous catalyst can be reused without losing its catalytic activity, making the industrial process more efficient, cheaper, and generating less waste [7,23]. Supports structural, mechanical, chemical, and thermal properties should be explored to increase the DMC yield by

assisting the catalytic system [2,7,23,37,49].

The high porosity of activated carbon fosters metal anchoring facilitating impregnation and making it an extremely efficient heterogeneous catalyst. Our group evaluated the use of activated carbon impregnated with iron, copper, nickel, and magnesium in DMC direct synthesis obtaining a yield of 23.5% with 100% selectivity [23].

Here we report the evaluation of the catalytic activity of metals (iron and copper) supported in different solids (silica, alumina, and eggshell waste) in the DMC direct synthesis and also the characterization of the pristine and metal-impregnated supports by TGA, BET, SEM-FEG, EDS mapping, XRD and DTP-NH<sub>3</sub> analysis.

## 2. Methodology

### 2.1. Materials

Methanol (>99.9% - EMSURE®), CH<sub>3</sub>OK (>95% - ALDRICH), iodomethane (>99.5% - ALDRICH), diethyl ether (>99.9% - EMSURE®), dimethylcarbonate - DMC (> 99.5% - ALDRICH), iron (III) nitrate nonahydrate (> 98.5% - ALDRICH), copper (II) nitrate trihydrate (> 99.0% - ALDRICH), alumina-AL (AL-Corp), silica-SI (SI-Corp), eggshell-ES waste, pearl-shaped molecular sieves (3A - ALDRICH), and CO<sub>2</sub> (99,8% - White Martins).

### 2.2. Synthesis of metallic catalysts by the impregnation method in substrates

The evaporative impregnation method is a straightforward technique used to enhance the impregnation yield of metallic catalysts by effectively adsorbing metals into the structure of porous materials. This method is particularly useful due to its simplicity in keeping metals within the porous matrix, allowing for efficient synthesis of metallic catalysts [23]. A solution containing 10 g of the support material (SI/AL/ES) and 1.7 g of different metal nitrates (iron and copper) in 250 mL of distilled water was prepared. The solution was kept under constant agitation at a temperature of 60 °C for 24 h, then placed in an oven at 100 °C overnight and, finally, calcined at 600 °C for 3 h. To use the eggshell as a support for the metals, a previous preparation was carried out using an oven at 100 °C for 24 h for drying and subsequent maceration and calcination (3 h at 600 °C) of the material to facilitate impregnation.

### 2.3. Characterization of supported metal ions

#### 2.3.1. Thermogravimetric analysis (TGA)

TA Instruments model Q600 equipment was used to perform the thermogravimetric analysis (TGA). A range of temperature from room to 1000 °C, with a heating rate of 20 °C/min under a synthetic air atmosphere was used. The actual metal impregnation (%) in the support was calculated according to Eq. (1), where the percentage of impregnation is given by the difference between the metal impregnated support (X-Y) sample weight and the weight of the pure support (X) sample in the temperature range of 25–1000 °C.

$$\% = (wt\%XY_{25-1000^{\circ}C}) - (wt\%X_{25-1000^{\circ}C}) \quad (1)$$

#### 2.3.2. Scanning electron microscopy with field emission (SEM-FEG)

FEI Inspect F50 equipment in the mode of secondary electrons (SE)

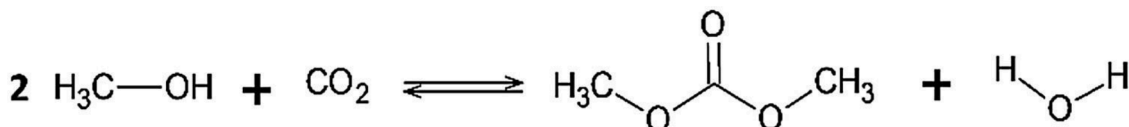


Fig. 1. DMC direct synthesis.

was used to perform the Scanning Electron Microscopy with Field Emission (SEM-FEG) analysis. Films were placed in a stub and covered with a thin layer of gold.

### 2.3.3. BET

The specific surface area was determined using the Brunauer-Emmet-Teller (BET) method, while the pore size and pore volume were calculated using the Barret-Joyner-Halenda method. The QUANTACHROME INSTRUMENTS model N42-28E with S/W code version 11.04 was utilized for these measurements. Before analysis, all samples were subjected to degassing at 150 °C for a minimum of 3 h.

### 2.3.4. FTIR-UATR

Infrared spectroscopy technique using a Perkin - Elmer 100 Spectrum at wavenumber range 4000–650 $\text{cm}^{-1}$  equipped with UATR (universal attenuated total reflectance) accessory was used to assess the chemical structure of supported catalysts and pristine supports. All samples were analyzed in the form of powder.

### 2.3.5. XRD

Shimadzu model XRD 7000 (X-Ray Powder Diffraction) equipment was used to perform the XRD analysis. Samples were placed in the equipment sample holder and analyzed between 2 and 70° (the region where the most intense peaks can appear). Parallel geometry support was used for the surface analysis. Copper k alpha radiation was used for analysis.

### 2.3.6. TPD-NH<sub>3</sub>

To determine the acid site distribution on synthesized catalysts, temperature-programmed desorption of NH<sub>3</sub> (NH<sub>3</sub>-TPD) was performed using Chemisorption Analyzer, Nanos ORD made by Sensiran Co., Iran. Catalyst (0.05 g) was placed in the measurement cell and degassed at 300 °C at a heat rate of 10 °C.min<sup>-1</sup> for 30 min, under 10 cm<sup>3</sup>.min<sup>-1</sup> helium gas flow. After that, the catalyst was cooled down to 110 °C and stabilized for 10 min. To begin the process, a stream of 5 wt% NH<sub>3</sub> with high-purity Helium as carrier gas with a flow rate of 10 mL.min<sup>-1</sup> was introduced for 30 min. To remove the physically adsorbed NH<sub>3</sub>, the carrier gas was switched to Helium and held for 1 h. The temperature was programmed to 800 °C with a heat rate of 10 °C.min<sup>-1</sup> for the desorption process.

## 2.4. DMC synthesis

A titanium alloy reactor (120 ml) with constant magnetic stirring was used to perform the experiments. A thermocouple connected to a temperature controller was used to keep the temperature steady using a resistive thermal band. Molecular sieves were placed in metallic compartment support in the gas phase [23,24]. For a typical reaction, 213 mmol of methanol, 0.7 g metal-impregnated ES/SI/AL, 20 mmol of CH<sub>3</sub>I, 2.0 g of molecular sieves, and 40 bar of CO<sub>2</sub> were used. The reactor was pressurized with CO<sub>2</sub> at 40 bar and heated at 80 °C. At the end of the reaction, the reactor was cooled to room temperature and then placed in an ice bath and slowly depressurized to collect DMC samples. Finally, an analysis of 3 recycles was performed using the best catalyst supported on the eggshell. After each reaction, the catalyst was washed several times in methanol and dried in an oven overnight. Catalyst reuse evaluation was performed using 213 mmol of methanol, 0.7 g metal-impregnated activated carbon, 20 mmol of CH<sub>3</sub>I, 2.0 g of molecular sieves (drying agent), 40 bar of CO<sub>2</sub> and 80 °C of temperature.

Gas Chromatograph (GC) Shimadzu GC-2014 with SH-Rtx-5 column and the programming of 31 °C for 0.5 min, rate of 10 °C / min to 50 °C for one minute, rate of 20 °C / min to 100 °C for 2 min and rate of 50 °C / min to 220 °C for 2 min was used to determine yield, conversion, and selectivity. All reaction tests were performed in triplicate. For the analysis, the samples were diluted with a concentration of 4% (v/v) in ethyl ether and injected into the GC to determine the DMC peak area

(2.4–2.7 min). Conversion, selectivity, and yield were calculated according to Faria et al. [24].

Methanol conversion was calculated using Eq. (2):

$$\text{conversion}(\%) = ((\text{reacted}) / (\text{total})) \times 100 \quad (2)$$

DMC selectivity was obtained by Eq. (3):

$$\text{selectivity}(\%) = ((\text{DMC}) / (\text{DMC} + (\text{by-products}))) \times 100 \quad (3)$$

DMC yield was determined using Eq. (4):

$$\text{yield}(\%) = ((\text{conversion}(\%) \times (\text{selectivity}(\%))) / 100) \quad (4)$$

## 2.5. Statistical analysis

Statistical analyses were performed using Minitab 18 Statistical Software-ANOVA aiming to assess the test's standard deviations (performed in triplicate) and analyze the Tukey test with 95% reliability. Equal letters show statistical equality between the sample averages.

## 2.6. Ab initio computer modeling

The electronic-structure calculations were carried out using plane-wave Kohn-Sham density functional theory (PW-KSDFT). The pure exchange-correlation functional proposed by Perdew, Burke, and Ernzerhof (PBE) [65] was used. The dispersion forces were added after each converged self-consistent field procedure. The molecular mechanics damped set of parameters known as D3 provided by Grimme and coworkers was used [70].

The non-valence electrons of all atoms were simulated utilizing the projector augmented3-wave method [8,18]. The application of periodic conditions to the atomic nuclei and electronic wave functions allows the simulation of virtually infinite systems. Such a setup eliminates undesirable boundary effects when describing the surface of the support. In all reported calculations, the adiabatic approximation applies.

The sizes of the simulation boxes were dictated by the sizes of the supercells of each support. The most energetically favorable arrangements of atoms were used based on the energy above the convex hull [36]. The chosen crystal system of Al<sub>2</sub>O<sub>3</sub> was trigonal, the crystal system of SiO<sub>2</sub> was tetragonal, the crystal system of CaO was cubic, and the crystal system of CaCO<sub>3</sub> was monoclinic. The constructed periodic (infinite) supercells including the surface, the d-metal atoms, and the adsorbed methanol molecule contained 68 atoms in the case of Al<sub>2</sub>O<sub>3</sub> support, 48 atoms in the case of SiO<sub>2</sub> support, 68 atoms in the case of CaO support, and 68 atoms in the case of CaCO<sub>3</sub> support. The k-point meshes of 2 × 2 × 1 were used to obtain more accurate electronic structures of the simulated surfaces.

The reaction barrier heights, transition states, and reaction thermochemistry were evaluated through the climbing image nudged elastic band approach (CI-NEB). The sixteen images were used to sample every chemical transformation including the first (reactants) and last (products) stationary points. All geometries were unrestricted during the simulations. The climbing image was identified on the fly at every iteration of the NEB algorithm. The harmonic force constants were set to equal numbers, 0.5 a.u., irrespective of the simulated system and normal forces induced by atoms [30,36].

The plane energy cut-off for the periodic wave functions was set to 700 eV in all systems for ease of comparison. The charge density energy cut-off was set to 2 800 eV. The wave function convergence threshold equaled 10<sup>-6</sup> Hartree. The geometry convergence threshold equaled 10<sup>-3</sup> a.u. The elastic band convergence threshold equaled 1.0 eV nm<sup>-1</sup>. The Quantum Espresso (version 6.5) PWSCF package6 was used to locate the stationary points and step-wise propagate the coordinates of the nudged elastic band [30].

### 3. Results

#### 3.1. Characterization of pristine and metal-impregnated supports

##### 3.1.1. TGA

Fig. 2 presents non-impregnated and metal-impregnated supports TGA analysis. For pristine SI and iron and copper-impregnated SI (SI-Fe and SI-Cu) (Fig. 2a), a single degradation step occurred related to silica structure moisture loss (temperatures below 150 °C) [38,68]. Pristine SI evidenced a total mass loss of ~7% and SI-Fe and SI-Cu of ~2%. Thus, one can infer the impregnated metal in SI-Fe of ~4% and SI-Cu of ~3%.

For alumina (AL) (Fig. 2b), two degradation steps were observed, the first at 100 °C (moisture loss), and the second near 400 °C attributed to

boehmite to  $\gamma$ -alumina phase change.<sup>50,51</sup> Metal impregnation is ~6% for AL-Fe and ~3% for AL-Cu.

For pristine ES and metal-impregnated ES (Fig. 2c), a single degradation step occurred at ~700 °C. It attributes to carbon dioxide loss. A slight mass loss was observed between 38 °C and 600 °C attributed to water and organic compounds present in the eggshell. Metal impregnation was ~13% for ES-Fe and ~7% for ES-Cu [29].

All supports presented metals impregnated in their structure, however, the support with greater impregnation of both metals was the eggshell residue (ES). The impregnation of iron in the supports was in the following order: ES-Fe (13%) > AL-Fe (6%) > SI-Fe (4%), and copper ES-Cu (7%) > AL-Cu (3%) = SI-Cu (3%).

##### 3.1.2. EDS e mapping

The chemical composition of pristine supports and metal-impregnated supports was obtained by EDS. Metal distribution was inferred by metal mapping (Figs. S1–S8 Supplementary Material).

AL, SI, and ES presented aluminum/oxygen, silica/oxygen, and calcium/oxygen, respectively. EDS analysis is semi-quantitative being possible to corroborate metal presence. AL, SI, and ES porosity is inhomogeneous over the entire surface interfering in metals dispersion and consequently in EDS analysis<sup>53–55</sup>. Yet, the eggshell has a greater number of mesopores. The metals are distributed on the surface and also inside pore structures [16,29,45].

##### 3.1.3. SEM-FEG

Fig. 3 shows SEM images of pristine and metal-impregnated SI, AL, and ES. As seen SI, AL, and ES present porosity, important for metal impregnation.

In Fig. 3- A, B and C we have the structure of SI, SI-Fe and SI-Cu, respectively, we can see in B and C the presence of metallic particles from the impregnation process. Silica may have channels in its structure that accommodate metals and provide greater catalytic activity due to easy diffusion between reactants and products [4,62,77,79].

In samples D, E and F, we have alumina, which is composed of leaf particles containing  $\gamma$ -Al<sub>2</sub>O<sub>3</sub> crystals, which with increasing temperature can undergo a transition to  $\theta$ -Al<sub>2</sub>O<sub>3</sub> and form  $\alpha$ -Al<sub>2</sub>O<sub>3</sub> crystals containing metals anchored in their surface [9,37].

SEM image of pristine ES (Fig. 3G) presents a porous structure. The fact that it has a more porous structure affects the amount of micropores and mesopores existing in its morphology, creating channels that allow the passage of CO<sub>2</sub> and facilitate the synthesis of DMC.

When iron or copper nitrate was added (Fig. 3H and I) the metal anchoring was performed in the elevations and porous regions as well as inside the channels changing surface morphology [16,45].

##### 3.1.4. BET

Specific surface area, pore volume, and pore radius are important to determine the material's ability to impregnate metal ions used as catalysts in the direct synthesis of DMC [50,79]. Table 1 presents the specific surface area, pore volume, and pore radius of samples.

Pristine ES presents a specific surface area of approximately 631 m<sup>2</sup>/g, pore volume of 0.27 cm<sup>3</sup>/g, and pore radius of 4.4 nm. SI shows a similar specific surface area of 603 m<sup>2</sup>/g, pore volume of 0.83 cm<sup>3</sup>/g, and pore radius of 2.7 nm. Unlike ES and SI, AL showed an inferior surface area of 152 m<sup>2</sup>/g, pore volume of 0.30 cm<sup>3</sup>/g, and pore radius of 3.4 nm.

When impregnated with iron ES increases its specific surface area, pore volume, and pore radius (780 m<sup>2</sup>/g, 0.31 cm<sup>3</sup>/g, and 4.6 nm). The same behavior was observed with copper (743 m<sup>2</sup>/g, 0.32 cm<sup>3</sup>/g, and 4.5 nm). The important increase in the specific surface area may be related to the larger pore radius compared to SI and AL. These values indicate that no pore blocking is occurring by metal ions instead a metal impregnation inside the pore structure occurred [7,86].

SI suffered a slight structural change with metal impregnation with both copper nitrate and iron nitrate (SI-Cu: 600 m<sup>2</sup>/g, 0.82 cm<sup>3</sup>/g e and

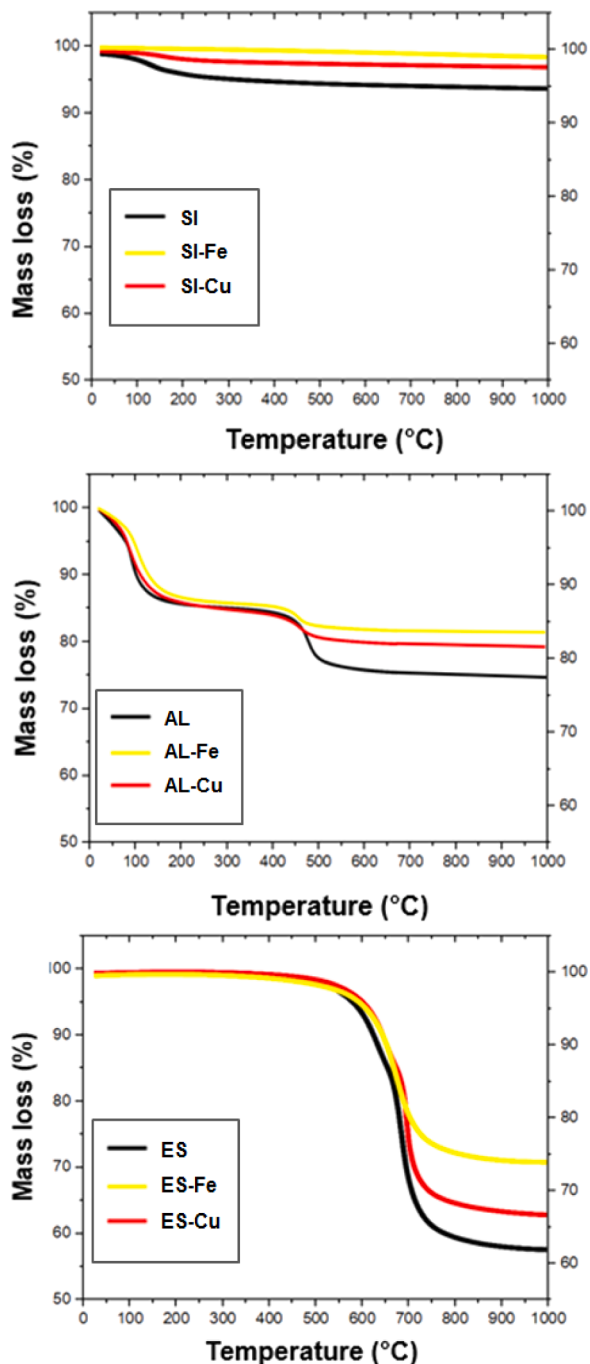


Fig. 2. TGA of samples: (a) SI/SI-Fe/SI-Cu; (b) AL/AL-Fe/AL-Cu; (c) ES/ES-Fe/ES-Cu.

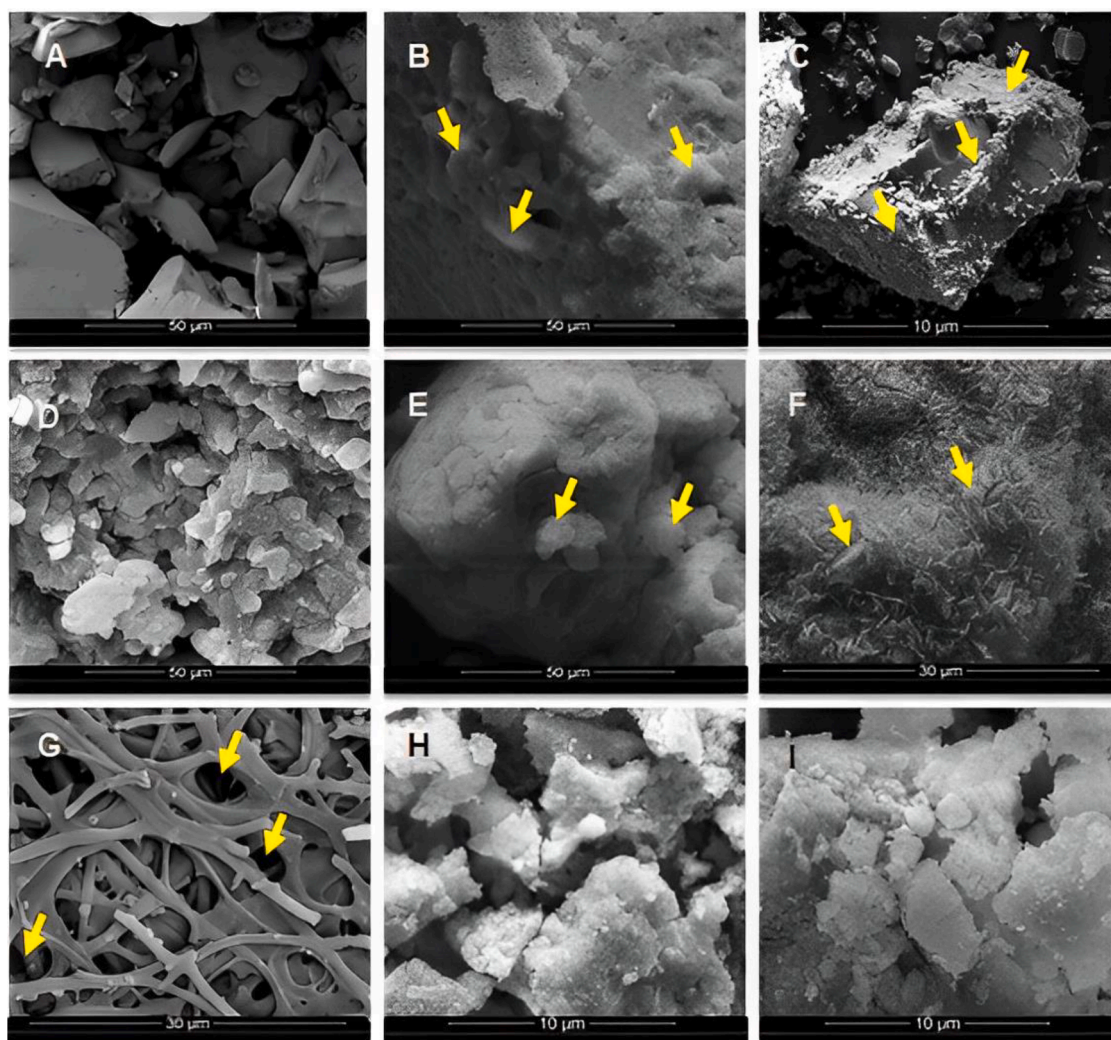


Fig. 3. SEM of supports impregnated with iron or copper: A: SI; B: SI-Fe; C: SI-Cu; D: AL; E: AL-Fe; F: AL-Cu; G: ES; H: ES-Fe; I: ES-Cu.

Table 1

BET surface areas, volume, pore radius of pristine support, and copper and iron-impregnated samples.

Sample	BET ( $\text{m}^2/\text{g}$ )	Pore Volume ( $\text{cm}^3/\text{g}$ )	Average pore radius (nm)
SI	603	0.83	2.7
SI-Fe	567	0.79	2.8
SI-Cu	600	0.82	2.7
AL	152	0.30	3.4
AL-Fe	201	0.32	3.2
AL-Cu	228	0.42	3.7
ES	631	0.27	4.4
ES-Fe	780	0.31	4.6
ES-Cu	743	0.32	4.5

2.7 nm; SI-Fe:  $567 \text{ m}^2/\text{g}$ ,  $0.79 \text{ cm}^3/\text{g}$  e and 2.8 nm). The same behavior was observed for AL (AL-Cu:  $228 \text{ m}^2/\text{g}$ ,  $0.42 \text{ cm}^3/\text{g}$  e and 3.7 nm; AL-Fe:  $201 \text{ m}^2/\text{g}$ ,  $0.32 \text{ cm}^3/\text{g}$  e and 3.2 nm).

Material calcination temperature is a very important factor affecting its specific surface area. Copper impregnation on silica at temperatures above  $600 \text{ }^\circ\text{C}$  could cause a large decrease in surface area [57], affecting the porosity and, consequently, impairing metal impregnation in its structure, resulting in a decrease in catalytic activity.

Several studies analyzed the use of different supports to impregnate metal ions, concluding that the support porosity increases the catalytic activity and allows the reuse of supported catalysts [52,96]. Some

studies ranked metal impregnation efficiency in different supports as a function of their porosity, reaching the following order: activated carbon > alumina > zeolite > silica [40,74]. In this study, we noticed that the more porous the material the greater the metal impregnation.

The use of residues such as eggshells has drawn attention due to their high porosity and ability to impregnate metal ions. According to Gao and Xu [29], the eggshell calcium carbonate is decomposed into calcium oxide during calcination and this change in composition leads to a structure homogenization, increasing the BET area and allowing greater metal ions impregnation.

The impregnation of metals in highly porous materials presents a multitude of advantages. Firstly, it promotes a more uniform distribution of metallic particles within the support's pores, leading to improved catalytic activity. Furthermore, this process enhances the mechanical properties of the materials, ensuring durability and an extended useful life. However, it is worth noting that when metals are impregnated into supports such as silica and alumina, the occurrence of surface compounds is possible. This phenomenon is commonly observed in situations where the materials experience cracking, resulting in the formation of highly acidic surface complexes [82].

Heat treatments applied to supports for metal impregnation induce significant structural transformations in solids. Generally, these treatments result in the growth of small crystals into larger ones, the transformation of amorphous solids into crystalline structures, and the agglomeration of small amorphous particles into larger ones. These

transformations play a crucial role in facilitating the impregnation of metals throughout the surface and pores of the supports. During thermal processes, if the solid's structure remains unchanged, it tends to evolve towards a state of lower surface free energy. Conversely, if modifications occur, a strongly exothermic transformation is necessary to counterbalance the substantial decrease in entropy resulting from the structural reorganization. The calcination step, involving higher temperatures, introduces porosity and enhances the mechanical strength of the material. It also triggers chemical reactions such as thermal decomposition of active agents, leading to the release of gasses. This gas evolution contributes to the development of greater porosity within the support. However, it's important to note that sintering, which involves the fusion of smaller particles into larger ones, can occur during the heat treatment process. This phenomenon can lead to a reduction in pore volume. Overall, by carefully considering the heat treatment conditions and balancing the competing factors of surface energy, entropy, and structural changes, it is possible to optimize the impregnation process and achieve desired properties in the final material [3,63].

The choice of calcination temperature significantly influences the texture and basicity properties of eggshell-based supports. Increasing the calcination temperature leads to the enlargement of support pores, resulting in a larger surface area and facilitating enhanced metal impregnation. Moreover, calcination at higher temperatures, typically around 900 °C, promotes the decomposition of CaCO<sub>3</sub> into CaO and CO<sub>2</sub>, thereby increasing the catalyst's basicity. However, it is crucial to optimize the calcination temperature to avoid potential drawbacks. Extreme temperatures can lead to the collapse of formed pores,

adversely affecting the overall support structure and, consequently, diminishing the catalytic activity's efficiency. Therefore, finding the balance in calcination temperature is vital to ensure the desired properties of the eggshell-based support without compromising its structural integrity. By carefully controlling the calcination temperature, it is possible to achieve the desired textural characteristics, such as pore size and surface area, as well as enhance the basicity of the catalyst. This optimization process ensures the effectiveness of the support for metal impregnation and subsequent catalytic applications [98].

### 3.1.5. FTIR

The FTIR analyses referring to the pristine and impregnated samples are shown in Fig. 4.

SI and AL showed bands around 3500cm<sup>-1</sup> attributed to the OH (hydroxyl) groups being less intense in pristine samples [23]. SI, SI-Fe, SI-Cu, AL, AL-Fe, and AL-Cu presented a band between 1000–1250 cm<sup>-1</sup> indicating C–O bonds present in sample structures [9,47,61,86,91]. In the silica supports SI, SI-Fe, AL-Fe, and SI-Cu a band between 1500–1600 cm<sup>-1</sup> attributed to C = C bonds is evidenced [10,47,57].

ES, ES-Fe, and ES-Cu presented similar bands at 1400, 900, 550, and 450 cm<sup>-1</sup>. The band around 1400 cm<sup>-1</sup> indicates the presence of Fe<sub>3</sub>O<sub>4</sub>.<sup>42</sup> The band at 1000 cm<sup>-1</sup> corresponds to CaO from CaCO<sub>3</sub> transformation at high temperatures. The bands at 500cm<sup>-1</sup> and 450cm<sup>-1</sup> reflect the presence of iron oxide in the support structure [16,45].

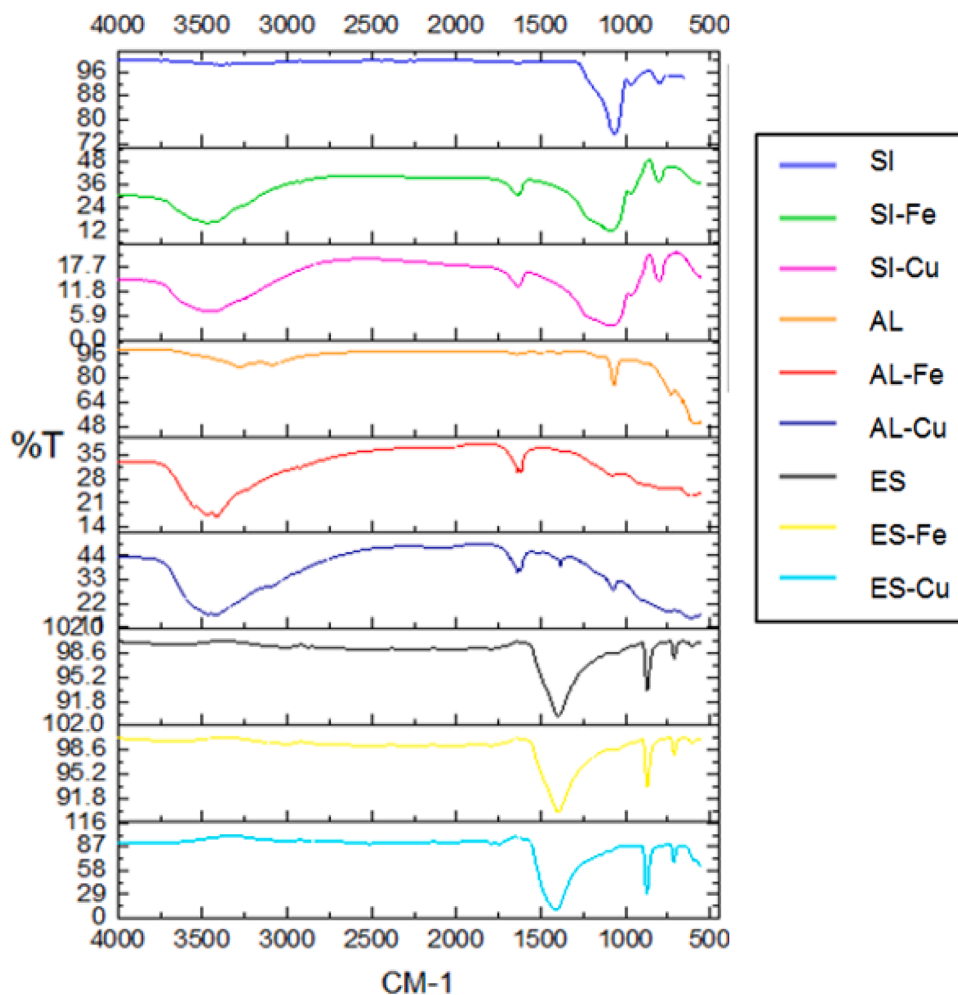


Fig. 4. FTIR spectra for pure and metal-impregnated supports.

### 3.1.6. XRD

For ES, ES-Fe, and ES-Cu a peak around 30° refers to the calcium carbonate contained in the samples (JCPDS 85–1108). Iron has characteristic peaks close to 30°, 35°, 45°, and 65° (JCPDS 82–1533 and 87–0121), whereas copper peaks appear around 42°, 50°, and 75° (JCPDS 003–1018) (see Fig S9, S10 and S11)

SI, SI-Fe, and SI-Cu show no difference in the XRD analysis (See Fig S12) presenting only one peak around 22.0°, which may refer to the tetrahedral units SiO<sub>4</sub> randomly distributed and joined by siloxane bridges (Si-O-Si), in addition to vicinal (Si-OH) and geminal (HO-Si-OH) silanol groups, all dispersed on the surface and sensitive to reactions that enable structural chemical changes [6,77].

For alumina, the sample peaks at 15, 30, 40, 50, and 65 °C appeared. All of them are characteristic of alumina (JCPDS 10–0425). For samples containing iron/copper, a peak around 45 °C appeared. It refers to iron nitrate (JCPDS 44–0520) and copper nitrate (JCPDS 85–1326).

### 3.1.7. DTP-NH<sub>3</sub>

The analysis of DTP-NH<sub>3</sub> allows inferring acidic sites present in the material structure. The number of acid sites present on the catalyst surface is proportional to the number of NH<sub>3</sub> adsorbed during the analysis.

Fig. 5 shows the DTP-NH<sub>3</sub> for all samples analyzed.

ES-Fe and ES-Cu present a desorbed NH<sub>3</sub> band around 700–750 °C indicating the presence of strong acid sites due to the elevated temperature needed for the desorption to occur [56]. For pristine ES the desorption band is undefined indicating the need of higher temperatures.

SI, SI-Fe and SI-Cu present a well-defined band at 100 °C, indicating the presence of a weak acid site. SI presents an intermediate acid site at 400 °C and, SI-Fe and SI-Cu at 450 °C, indicating a slight increase in temperature. The increase in the area of the band for samples impregnated with metals indicates the increase in the acid sites number [15,44,56,97].

AL presents a different NH<sub>3</sub> desorption band profile when compared to samples impregnated with metals. For AL a desorption band at 500 °C is seen while metal-impregnated samples present well-defined bands at 200 °C indicating weaker acid sites [15,44]. AL-Fe presents a desorption band at 600 °C indicating the present of a strong acid site.

The formation of DMC increases in the presence of catalysts with acidic and basic sites in their structure [41,55,59,85,99]. Both basicity and acidity enhance catalytic action, causing a synergistic effect on the catalytic and DMC formation process [25,32,41,69]. Literature describes strong basic sites in eggshell-containing catalysts, as shown by TPD-CO<sub>2</sub> analyses [25].

### 3.2. Application of catalysts (X-Y) in the direct synthesis of dimethyl carbonate (DMC)

The conversions, yields, selectivities, and water content of the reactions using the supported catalysts are presented in Table 2.

For pristine SI, AL, and ES (Entry 1, Entry 4, and Entry 7) only product traces were evidenced with >99% selectivity. Low conversion using pure supports may indicate a low concentration of metals already present in the supports before iron and copper impregnation.

Regarding the copper/support as a catalyst, we noticed that ES

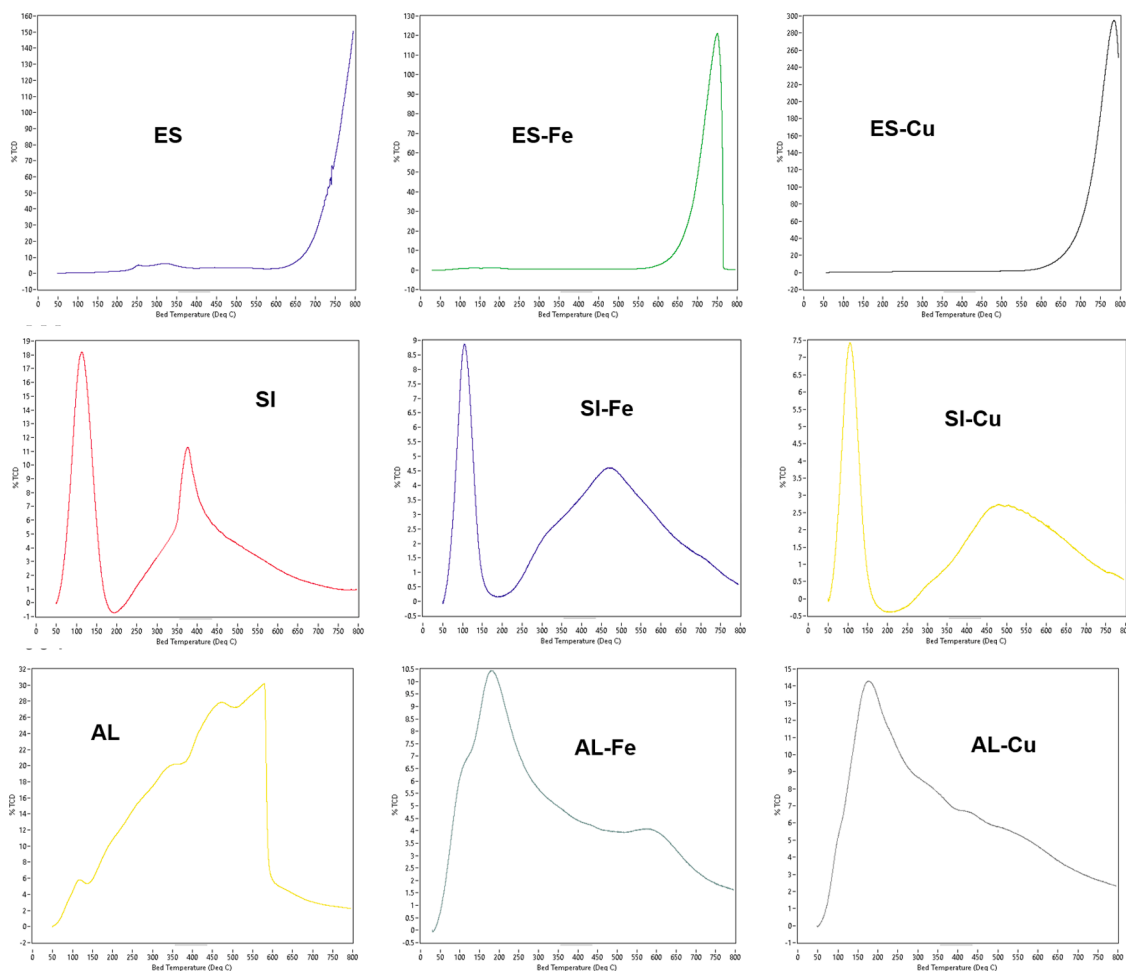


Fig. 5. DTP-NH<sub>3</sub> of pristine supports (X) and samples X-Y.

**Table 2**

Conversion, yield, selectivity, and water content of reactions with catalysts (X-Y).

Entry	Catalyst	Selectivity (%)	Conversion (%)	Yield(%)	Water (%)
1	SI	>99	TRACES	TRACES	TRACES
2	SI-Fe	>99	7.2 ± 1.7	7.2 ± 1.7 <sup>a</sup>	0.5 ± 0.1
3	SI-Cu	>99	6.2 ± 1.2	6.2 ± 1.1 <sup>a</sup>	1.4 ± 0.9
4	AL	>99	TRACES	TRACES	TRACES
5	AL-Fe	>99	7.0 ± 0.9	7.0 ± 0.9 <sup>ab</sup>	1.7 ± 1.0
6	AL-Cu	>99	4.8 ± 0.8	4.8 ± 0.8 <sup>ac</sup>	1.9 ± 0.9
7	ES	>99	TRACES	TRACES	TRACES
8	ES-Fe	>99	12.7 ± 0.5	12.7 ± 0.5 <sup>c</sup>	0.9 ± 0.5
9	ES-Cu	>99	11.3 ± 0.7	11.3 ± 0.7 <sup>d</sup>	1.1 ± 0.2

\*The letters present next to the yield refer to the Tukey test performed to define statistical equality between the samples. \*\*Pressure: 40 bar; Temperature: 80 °C; Time: 24 h; 0.7 g of X-Y; 2.0 g of molecular sieve; 213 mmol methanol; 20 mmol of CH<sub>3</sub>I.

proved to be the most active, reaching a yield of approximately 11.3% (Entry 9), followed by AL with 8.9% (Entry 6) and SI with 6.2% (Entry 3). The best performance of ES can be attributed to the presence of a more acid sites and porous structure with larger porous facilitating copper impregnation and the conversion to DMC.

Gao and Xu [29] studied the transesterification of propylene carbonate and methanol using eggshells as catalysts. The propylene carbonate conversion and the DMC yield reached maximum values after 1 h (80 and 75%, respectively) under the optimal conditions (methanol/propylene carbonate molar ratio 10:1, 0.8% by weight of the eggshell catalyst, room temperature, and 1 atm pressure). In addition, the eggshell catalyst can be reused in four cycles with light deactivation. The eggshell showed catalytic behavior similar to pure CaO. Calcium carbonate from the eggshell is decomposed into calcium oxide during calcination and this change in composition leads to a homogenization of the structure increasing the BET area and producing an effective solid renewable catalyst.

When comparing the iron/support as a catalyst, ES also proved to be more efficient, reaching around 12.7% conversion and >99% selectivity (Entry 8). SI-Fe showed a yield of 7.2% and AL-Fe 6.1% both with >99% selectivity. Li et al. [51] evaluated the combination of iron with zirconia in the direct synthesis of DMC (110 °C, 5Mpa, and 4 h of reaction time) in different proportions and concluded that the increase in the number of iron particles results in higher conversion and yield. The use of Fe<sub>0.7</sub>Zr<sub>0.3</sub>O<sub>y</sub> as a catalyst provided a yield of approximately 4% and a selectivity of 100%. The combination of zirconia with iron was fundamental to increasing yield and selectivity since the pristine support showed no catalytic activity.

For AL and SI, the supports act differently depending on the impregnated metal. Regarding Fe impregnation, AL and SI showed the same catalytic efficiency as a function of Tukey's test and standard deviation interval (Entry 3 and 6) and SI was superior to AL when impregnated with iron (Entry 2 and 5). On the other hand, ES was superior to other supports, both ES-Fe and ES-Cu. However, ES-Fe achieved a conversion of approximately 10% higher than ES-Cu in the DMC direct synthesis. Tukey test proved that the samples with the best results (ES-Fe and ES-Cu) are statistically different from each other. In turn, SI-Fe and SI-Cu are similar.

Finally, we noticed that in both reactions, the water content in the product was small indicating the efficiency of the dehydrating agent, being the minimum for SI-Fe (0.5%) and the maximum for SI-Cu (1.4%). Small amounts of water produced during the reaction lead to an increase in the DMC yield, shifting reaction equilibrium to products. An efficient catalyst allied to a good dehydrating system improves the DMC direct synthesis, even if such synthesis presents unfavorable thermodynamics for the direct reaction.

The use of ES-Fe as catalyst for DMC direct synthesis showed the best conversion result (40 bar, 80 °C and 24 h). To compare our findings with

the literature, Table 3 presents results concerning the DMC yield, reaction parameters, catalyst synthesis methods, and specific surface area of catalysts in the direct synthesis of DMC.

Table 3 shows that different techniques can be used for the preparation of the catalysts for DMC obtainment resulting in different specific surface area properties and impregnation of metals on the surface. Xuan et al. [93] evaluated that the use of impregnation may have affected the dispersion of metals on the sample surface, influencing the available specific surface area due to the agglomeration of metals. The encapsulation technique was revisited aiming to improve the availability of porosity and the presence of metals homogeneously distributed in the catalyst surface. The vacancies and availability of acidic and basic sites are also important, since both have a great influence on the direct synthesis of DMC, accelerating the interactions between reagents and catalyst, increasing the yield, and, consequently, the selectivity of the product.

Faria et al. [23] conducted an evaluation on the utilization of activated carbon in conjunction with metals impregnated via the evaporative impregnation method. Their findings demonstrated that employing this technique resulted in an excellent yield of metals adsorbed onto the surface. The surface area of the pure support was initially measured at approximately 985 m<sup>2</sup>/g, but after impregnation, it decreased to 620 m<sup>2</sup>/g. This decrease in surface area indicated that the metals were effectively adsorbed onto the support structure. Additionally, the achieved results for DMC yield surpassed those of previous studies, reaching approximately 23.5% with a selectivity of 100%.

Superior or statistically equal results for DMC direct synthesis using ES-Fe, as described in this work, were obtained when compared with the results presented in Table 3. In addition, the synthesis is performed in milder conditions, reducing the energy spent on the entire system. The ES-Fe catalyst presented a balance between acidic and basic sites, which proved to be extremely important for achieving high yield. Since the matrix used is waste from the food industry, we still have the environmental issue, since the work values the use of waste for the synthesis of a product with high added value. Therefore, based on the best result, the catalyst was reused to assess whether the catalytic action would remain constant during 4 cycles.

### 3.2.1. Reuse of the catalyst ES-Fe

Fig. 6 shows the selectivity and conversion of ES-Fe catalyst in the direct synthesis of DMC.

Recycle number 0 represents the first use of ES-Fe as catalyst achieving 12.7% of conversion. Number 1 is the first reuse with a slight decrease in conversion reaching 11.3%. In the next reuses (numbers 2 and 3) the catalytic activity remained to decrease (9.3% and 5.2% of conversion, respectively) losing about 60% of the catalytic activity. Regarding the selectivities, no change was observed.

Eggshell-impregnated metal (TiO<sub>2</sub>) was used as catalyst in the synthesis of carbonates, such as glycerol carbonate, achieving high conversions and selectivities. Regarding reuse, the catalytic activity showed a great decrease from the 4th recycle, however, the selectivity remained stable during all reactions [66]. Eggshell was also tested as catalyst in the synthesis of carbonate from glycerol via transesterification of glycerol and DMC, with yields of up to 90% with 100% selectivity. The reuse evidenced an important decrease in the catalytic activity from the 3rd cycle when there was no calcination pre-treatment in the catalyst. When the catalyst was submitted to calcination carried out at 900 °C a continuous and stable catalytic activity was observed for 3 reuses [67].

The use of eggshell impregnated with iron presented an efficient catalytic activity in cycles 1 and 2, however, reuse number 3 indicates a drastic decrease in the catalytic activity of ES-Fe with a conversion of 5.2%. This behavior could be associated with the calcination process. Performing a calcination process at higher temperatures (~750–800 °C) could improve the catalytic activity but a higher energy expenditure for catalyst synthesis will be necessary.

**Table 3**

Results concerning the DMC yield, reaction parameters, catalyst synthesis methods, and specific surface area of catalysts in the direct synthesis of DMC.

Catalyst	Parameters to DMC synthesis	Preparation method of catalyst	Surface area ( $\text{m}^2\text{g}^{-1}$ )	DMC yield	Refs.
CeO <sub>2</sub>	5 h, 4.0 MPa, 140 °C	Simple hydrothermal method	137	~13.0% with 92.3% selectivity	[95]
ZrO <sub>2</sub>	170 °C, 70 h, 15 MPa, molecular sieves 3A (5.0 g)	Calcination and impregnation	110	1.0% with 100% selectivity	[101]
Ce/ZrO <sub>2</sub>			21	14.3 ± 2.3% with 100% selectivity	
HPW@MOF-808 (Encapsulating phosphotungstic acid within metal-organic framework)	140 °C, 4 h, 12 MPa	Simple encapsulation	285	4.65% with 100% selectivity	[93]
Activated carbon impregnated with iron (AC-Fe)	80 °C, 40 bar, 24 h, molecular sieves 3A (2.0 g)	Evaporation impregnation method	620	23.5 ± 0.8 with 100% selectivity	[23]

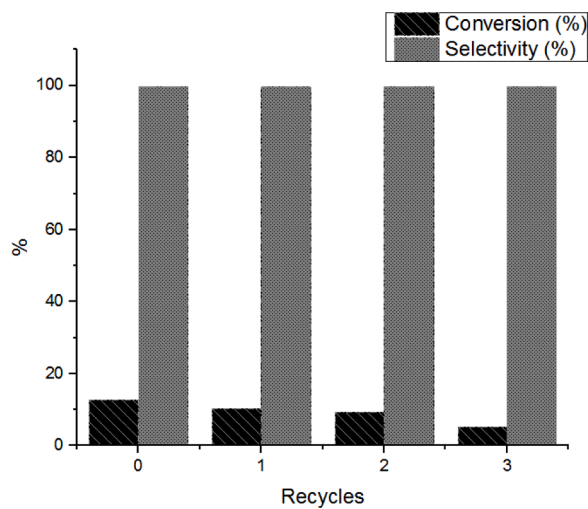


**Fig. 6.** Conversion and selectivity of DMC synthesis using Es-Fe catalyst. \*Pressure: 40 bar; Temperature: 80 °C; Time: 24 h; 0.7 g of ES-Fe; 2.0 g of molecular sieve; 213 mmol methanol; 20 mmol of CH<sub>3</sub>I.

### 3.3. Deprotonation of methanol by means of various catalysts and supports: *Ab initio* reaction paths

The considered synthesis of DMC begins with the adsorption of the methanol molecule on the catalytic surface. The oxygen atom of methanol coordinates D-metals and, therefore, becomes more polarized. The polarized oxygen-hydrogen covalent bond of methanol breaks apart as that of acid. The split-off proton joins one of the oxygen atoms belonging to the support surface nearby. The hydroxyl group appears on the support surface. Next, the CO<sub>2</sub> molecule attacks the CH<sub>3</sub>O\* moiety which remains electrostatically attracted by the D-metal atom. The methyl carbonate group, CH<sub>3</sub>-O-C(O)-O\* emerges. Eventually, the methyl radical of the CH<sub>3</sub>I attaches, and the DMC molecule forms. The iodide anion takes the proton from the surface of the support and produces HI. The catalytic cycle then repeats.

The characterization indicates the presence of hydroxyl groups in the system. In turn, the identification of the reaction products reveals a formation of non-negligible fractions of water. It is, therefore, a reasonable hypothesis that in certain cases the methanol's proton joins the hydroxyl group and gives rise to a water molecule. Due to the kinetic and thermodynamic stability of the water molecule, it does not undergo further chemical transformations. The drying agents were used to prevent this water from hydrolyzing DMC.

The most hindered stage of the DMC synthesis is the deprotonation of methanol (Fig. 7) which represents a very weak acid and fully blocks the reaction in the absence of the D-metal catalysts (Table 2). To unveil the activation barriers, we investigated the potential energy surface between the protonated and deprotonated forms of methanol by the NEB

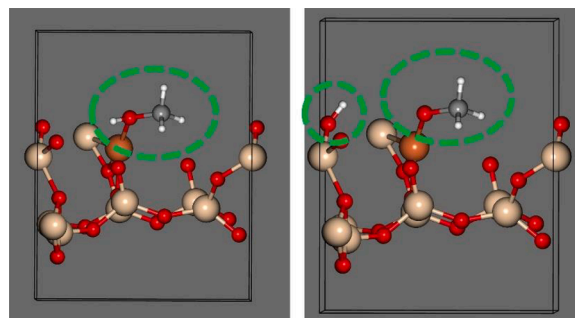


**Fig. 7.** (Right) The methanol molecule adsorbed at the infinite silica surface. (Left) Deprotonated methanol molecule passivated by the copper atom. Silicon is pale pink; oxygen is red; hydrogen is white; carbon is gray; copper is orange.

method. NEB finds a minimum energy path and saddle points between the reactants and the products provided that both are known.

The reaction paths are given in Fig. 8 providing respective activation barriers and energy effects of the considered reaction stage. The NEB method optimizes the virtual band (minimum reaction path) by simultaneously calculating forces acting on all atomic nuclei in all intermediate molecular configurations (so-called images). There are two types of forces in the systems, viz., the interatomic forces and the spring forces. Relative to the reaction path band, only the parallel components of the spring forces and the perpendicular components of the interatomic forces are accounted for. Note that the artificial spring forces are needed to adjust the spacing of the optimized images along the reaction path band. The resulting energetics of the simulated process reflects the true energy expenses of the system that undergoes alterations.

The methanol deprotonation reactions occur similarly in all eight considered samples. The transition states occur at the hydrogen-oxygen distances ranging between 0.123–0.130 nm and D-metal-oxygen distances ranging between 0.18 and 2.0 nm. The elongation of a covalent bond by approximately 30% during the course of the bond breaking event is a conventional physical behavior. As a result of deprotonation, the metal-oxygen distances shrink substantially. For instance, the iron (catalyst)-oxygen(methanol) distance equals 0.192 nm before the reaction and 0.175 nm after the reaction as adsorbed on the CaO support. Compare to the case of copper. The copper(catalyst)-oxygen(methanol) distance equals 0.204 nm before the reaction and 0.186 nm in the deprotonated state.

The simulated energetics appears to be in quite a decent agreement with the experimental conversions and yields (Table 2). We interpret such a good correlation of the obtained data as a paramount role of methanol deprotonation during the course of the methanol conversion into DMC. In all samples, the iron catalyst performs better compared to the copper catalyst. This trend should have been expected because iron is a more active metal. Iron polarizes the electron cloud of the oxygen atom of methanol to a larger extent than copper. Hence, the breakage of the oxygen-hydrogen covalent bond occurs easier. Both the energetic

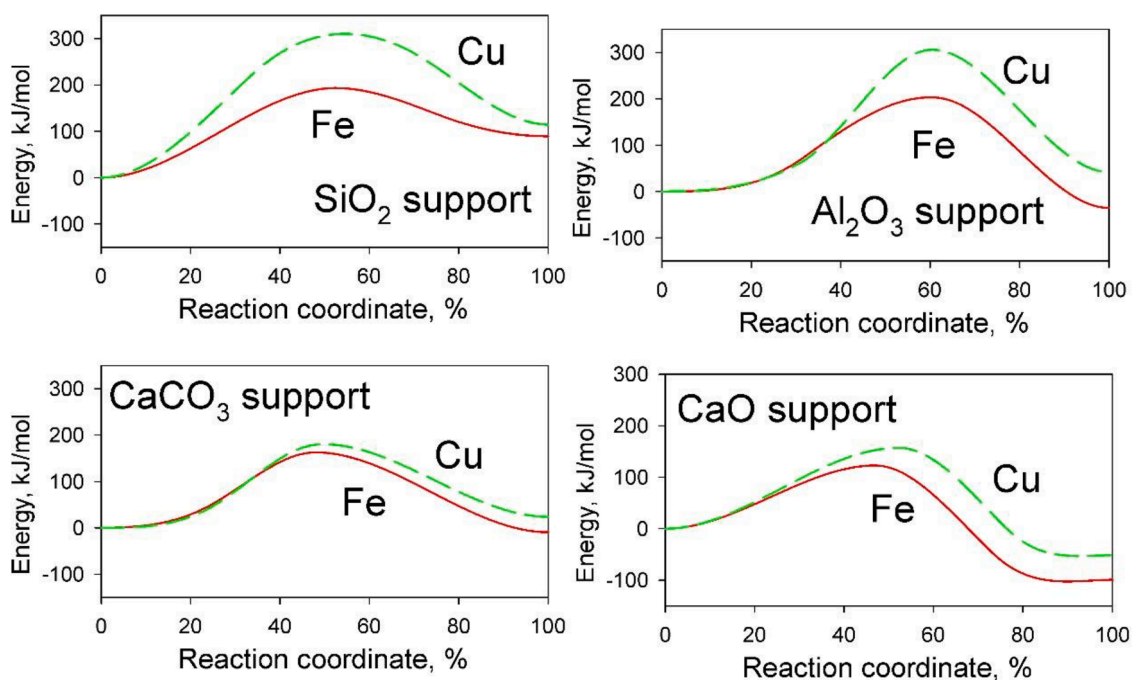


**Fig. 8.** The minimum reaction paths for the methanol deprotonation in various systems. Note that the depicted reaction coordinates represent collective variables reflecting all changes in the systems during the course of the reaction. The so-defined reaction coordinates cannot be linked to any specific components of the simulated Z-matrices. Based on their definition, the reaction coordinates are unique in all systems and cannot be directly compared.

effect of the reaction and the activation barrier height are smaller in the case of the iron catalyst than in the case of the copper catalyst. In practical applications, the iron catalyst must be preferred.

The support plays an essential role in the deprotonation of methanol. Indeed, the support directly interacts with the catalyst particle (iron or copper) and accepts the detached proton. Note that the recorded heights of the activation barriers are more essential parameters than the energy effects since the latter is largely compensated by subsequent stages. According to Hess's law, the energy effect does not depend on the reaction mechanism. In turn, the activation barrier determined the percentage of successful elementary reaction events and directly limits the conversions and yields.

The SI and AL supports exhibit similar performance in line with the recorded experimental descriptors of the corresponding chemical reactions. While the atoms in their structures possess high formal electrostatic charges (+4 on Si in  $\text{SiO}_2$  and +3 on Al in  $\text{Al}_2\text{O}_3$ ), an actual electronic density is strongly delocalized largely due to the small size of these formal ions. As a result, the SI and AL supports perform even worse than the ES support with a less delocalized positive electrostatic charge on Ca. In this respect, minimum reaction path simulations and experimental reaction studies confirm and supplement one another.

The CaO and  $\text{CaCO}_3$  surfaces constitute the ES support. A certain fraction of CaO is expected to form after the performed annealing to impregnate Fe and Cu catalysts. We anticipate that the precise ratio of the considered moieties depends on the conditions of annealing. In simulations, we considered CaO and  $\text{CaCO}_3$  independently to separate their effects within the experimental results. Interestingly, the CaO support performs somewhat better. Compare the barriers of 160 and 180 kJ/mol for Fe on  $\text{CaCO}_3$  and Cu on  $\text{CaCO}_3$  to the barriers of 130 and 150 kJ/mol CaO and Cu on CaO. The observed difference can be rationalized, as above, by a slightly more electron-deficient  $\text{Ca}^{2+}$  particle in CaO.

To recapitulate, the minimum reaction path simulations confirm a more efficient performance of more chemically active oxide-forming chemical elements. We hereby hypothesize that barium oxide and even barium superoxide can enhance the DMC yields and allow one to use milder reaction conditions. Recently, it was shown [12,22] that

potassium being even more active than Ca and Ba enhance methanol conversion into DMC a fewfold.

#### 4. Conclusions

The synthesis of DMC using a compound reaction presents significant challenges due to unfavorable thermochemistry and a high activation barrier. Catalysts, particularly D-metal oxide moieties, can enhance the reaction yield, but their effectiveness depends on the specific D-metal and support used. This study contributes to understanding the catalytic transformation of methanol and  $\text{CO}_2$  into DMC, as well as identifying more efficient reaction pathways. Comprehensive chemical characterization analyses confirm the successful impregnation of D-metal into the support structures, with eggshell waste demonstrating the highest percentage of D-metal and greater catalytic activity. The best results were achieved with the ES-Fe sample, which exhibited a methanol conversion of 12.7% and 100% selectivity, followed by the ES-Cu sample with a yield of 11.3% and 100% selectivity. The support material directly influences the catalytic performance, and the ES-Fe catalyst showed stability and high conversion and selectivity even after multiple reuses. This work contributes to the sustainable utilization of excessive  $\text{CO}_2$  by providing a methodology for producing DMC from  $\text{CO}_2$  and methanol using supported D-metal oxide catalysts. The insights gained from this study can guide the development of more robust catalytic systems and the binding of higher  $\text{CO}_2$  percentages.

#### 5. Future perspectives

The direct synthesis of DMC faces several challenges that require attention to improve the process. These challenges include unfavorable reaction thermodynamics, water production, and the search for catalysts to enhance yield and selectivity. The high temperatures required for the calcination process of the support pose an energy-demanding issue, which needs to be addressed for a low-carbon process. In our future perspectives, we aim to explore new low-energy processes for support production. Additionally, considering the influence of the support on reaction activity and selectivity, we plan to investigate the use of

lignocellulosic residues, such as rice husks and coffee husks, as potential supports for metal impregnation. This approach would provide a valuable application for these otherwise discarded residues in DMC synthesis, creating a high-value product. Another crucial aspect to be studied is the optimization of the process in larger-capacity reactors to evaluate reproducibility and assess the potential for industrial implementation.

## Declarations

### Ethical approval

Not applicable.

### Authors' contributions

All authors contributed to the study conception and design. Material preparation, data collection and analysis were performed by Douglas José Faria, Leonardo Moreira dos Santos and Vitaly Chaban. The first draft of the manuscript was written by Sandra Einloft, Douglas Farias and all authors commented on previous versions of the manuscript. All authors read, contributed, and approved the final manuscript.

### Funding

This study was financed by Petrobras and the Coordenação de Aperfeiçoamento de Pessoal de Nível Superior – Brasil (CAPES) – Finance Code 001.

### Availability of data and materials

All spectra data are included in the supplementary information file.

### Declaration of Competing Interest

The authors declare that they have no known competing financial interests or personal relationships that could have appeared to influence the work reported in this paper.

### Acknowledgments

Douglas Faria thanks CAPES; Sandra Einloft thanks CNPq for research scholarship. This study was financed in part by the Coordenação de Aperfeiçoamento de Pessoal de Nível Superior – Brasil (CAPES) – Finance Code 001. The authors thank Petrobras for financial support and the strategic importance of the support given by ANP (Brazil's National Oil, Natural Gas and Biofuels Agency) through the R&D levy regulation.

### Supplementary materials

Supplementary material associated with this article can be found, in the online version, at [doi:10.1016/j.molstruc.2023.136110](https://doi.org/10.1016/j.molstruc.2023.136110).

### References

- [1] K. Almusaiter, Synthesis of dimethyl carbonate (DMC) from methanol and CO<sub>2</sub> over Rh-supported catalysts, *Catal. Commun.* 10 (7) (2009) 1127–1131, <https://doi.org/10.1016/j.catcom.2009.01.012>.
- [2] A.S. Aquino, F.L. Bernard, J.v. Borges, L. Mafrá, F.D. Vecchia, M.O. Vieira, R. Ligabue, M. Seferin, V.V. Chaban, E.J. Cabrita, S. Einloft, Rationalizing the role of the anion in CO<sub>2</sub> capture and conversion using imidazolium-based ionic liquid modified mesoporous silica, *RSC Adv.* 5 (79) (2015), <https://doi.org/10.1039/C5RA07561K>.
- [3] H. Arai, M. Machida, Thermal stabilization of catalyst supports and their application to high-temperature catalytic combustion, *Appl. Catal. A* 138 (2) (1996) 161–176, [https://doi.org/10.1016/0926-860X\(95\)00294-4](https://doi.org/10.1016/0926-860X(95)00294-4).
- [4] L. Bai, H. Hu, W. Fu, J. Wan, X. Cheng, L. Zhuge, L. Xiong, Q. Chen, Synthesis of a novel silica-supported dithiocarbamate adsorbent and its properties for the removal of heavy metal ions, *J. Hazard. Mater.* 195 (2011) 261–275, <https://doi.org/10.1016/j.jhazmat.2011.08.038>.
- [5] D. Ballivet-Tkatchenko, S. Chambrey, R. Keiski, R. Ligabue, L. Plasseraud, P. Richard, H. Turunen, Direct synthesis of dimethyl carbonate with supercritical carbon dioxide: characterization of a key organotin oxide intermediate, *Catal. Today* 115 (1–4) (2006), <https://doi.org/10.1016/j.cattod.2006.02.025>.
- [6] H. Beidaghy Dizaji, T. Zeng, I. Hartmann, D. Enke, T. Schliermann, V. Lenz, M. Bidabadi, Generation of high quality biogenic silica by combustion of rice husk and rice straw combined with pre- and post-treatment strategies—a review, *Appl. Sci.* 9 (6) (2019), <https://doi.org/10.3390/app9061083>.
- [7] E. Blanco, C. Sepulveda, K. Cruces, J.L. García-Fierro, I.T. Ghampson, N. Escalona, Conversion of guaiacol over metal carbides supported on activated carbon catalysts, *Catal. Today* 356 (2020) 376–383, <https://doi.org/10.1016/j.cattod.2019.08.029>.
- [8] P.E. Blöchl, Projector augmented-wave method, *Phys. Rev. B* 50 (24) (1994) 17953–17979, <https://doi.org/10.1103/PhysRevB.50.17953>.
- [9] G.N. Bondarenko, E.G. Dvurechenskaya, O.G. Ganina, F. Alonso, I.P. Beletskaya, Solvent-free synthesis of cyclic carbonates from CO<sub>2</sub> and epoxides catalyzed by reusable alumina-supported zinc dichloride, *Appl. Catal. B* 254 (2019) 380–390, <https://doi.org/10.1016/j.apcatb.2019.04.024>.
- [10] E.A.D.F. Braga, A.C. Batista Junior, Modificação química de sílica gel obtida de areia e seu uso na remoção de Cu<sup>2+</sup>, Zn<sup>2+</sup>, Mn<sup>2+</sup>, *Eclét. Quím.* J. 41 (1) (2017) 85, <https://doi.org/10.26850/1678-4618eq.v41.1.2016.p85-93>.
- [11] Q. Cai, C. Jin, B. Lu, H. Tangbo, Y. Shan, Synthesis of dimethyl carbonate from methanol and carbon dioxide using potassium methoxide as catalyst under mild conditions, *Catal. Lett.* 103 (3–4) (2005), <https://doi.org/10.1007/s10562-005-7158-2>.
- [12] Q. Cai, C. Jin, B. Lu, H. Tangbo, Y. Shan, Synthesis of dimethyl carbonate from methanol and carbon dioxide using potassium methoxide as catalyst under mild conditions, *Catal. Lett.* 103 (3–4) (2005) 225–228, <https://doi.org/10.1007/s10562-005-7158-2>.
- [13] A.A. Chaugule, A.H. Tamboli, H. Kim, Ionic liquid as a catalyst for utilization of carbon dioxide to production of linear and cyclic carbonate, *Fuel* 200 (2017), <https://doi.org/10.1016/j.fuel.2017.03.077>.
- [14] P. Chen, S. Huang, J. Zhang, S. Wang, X. Ma, Enhanced CuCl dispersion by regulating acidity of MCM-41 for catalytic oxycarbonylation of ethanol to diethyl carbonate, *Front. Chem. Sci. Eng.* 9 (2) (2015) 224–231, <https://doi.org/10.1007/s11705-014-1447-5>.
- [15] Y. Chen, Y. Li, W. Chen, W.W. Xu, Z. Han, A. Waheed, Z. Ye, G. Li, A. Baiker, Continuous dimethyl carbonate synthesis from CO<sub>2</sub> and methanol over Bi<sub>2</sub>Ce<sub>1-x</sub>O<sub>6</sub> monoliths: effect of bismuth doping on population of oxygen vacancies, activity, and reaction pathway, *Nano Res.* 15 (2) (2022) 1366–1374, <https://doi.org/10.1007/s12274-021-3669-4>.
- [16] C. Chingakham, A. David, V. Sajith, Fe<sub>3</sub>O<sub>4</sub> nanoparticles impregnated eggshell as a novel catalyst for enhanced biodiesel production, *Chin. J. Chem. Eng.* 27 (11) (2019) 2835–2843, <https://doi.org/10.1016/j.cjche.2019.02.022>.
- [17] S. Cui, J. Borgemenke, Z. Liu, H.M. Keener, Y. Li, Innovative sustainable conversion from CO<sub>2</sub> and biodiesel-based crude glycerol waste to bio-based polycarbonates, *J. CO<sub>2</sub> Util.* 34 (2019) 198–206, <https://doi.org/10.1016/j.jcou.2019.06.004>.
- [18] A. Dal Corso, Pseudopotentials periodic table: from H to Pu, *Comput. Mater. Sci.* 95 (2014) 337–350, <https://doi.org/10.1016/j.commatsci.2014.07.043>.
- [19] D. Delledonne, F. Rivetti, U. Romano, Developments in the production and application of dimethylcarbonate, *Appl. Catal. A* 221 (1–2) (2001) 241–251, [https://doi.org/10.1016/S0926-860X\(01\)00796-7](https://doi.org/10.1016/S0926-860X(01)00796-7).
- [20] F. Dong, Y. Wang, B. Su, Y. Hua, Y. Zhang, The process of peak CO<sub>2</sub> emissions in developed economies: a perspective of industrialization and urbanization, *Resour. Conserv. Recycl.* 141 (2019), <https://doi.org/10.1016/j.resconrec.2018.10.010>.
- [21] A.O. Esan, A.D. Adeyemi, S. Ganesan, A review on the recent application of dimethyl carbonate in sustainable biodiesel production, *J. Clean. Prod.* 257 (2020), 120561, <https://doi.org/10.1016/j.jclepro.2020.120561>.
- [22] S. Fang, K. Fujimoto, Direct synthesis of dimethyl carbonate from carbon dioxide and methanol catalyzed by base, *Appl. Catal. A* 142 (1) (1996) L1–L3, [https://doi.org/10.1016/0926-860X\(96\)00081-6](https://doi.org/10.1016/0926-860X(96)00081-6).
- [23] D.J. Faria, L.M. dos Santos, F.L. Bernard, I.S. Pinto, I.P. Romero, V.V. Chaban, S. Einloft, Performance of supported metal catalysts in the dimethyl carbonate production by direct synthesis using CO<sub>2</sub> and methanol, *J. CO<sub>2</sub> Util.* 53 (2021), <https://doi.org/10.1016/j.jcou.2021.101721>.
- [24] D.J. Faria, L. Moreira dos Santos, F.L. Bernard, I. Selbach Pinto, M.A. Carmona da Motta Resende, S. Einloft, Dehydrating agent effect on the synthesis of dimethyl carbonate (DMC) directly from methanol and carbon dioxide, *RSC Adv.* 10 (57) (2020) 34895–34902, <https://doi.org/10.1039/D0RA06034H>.
- [25] M. Farooq, A. Ramli, M. Gul, A. Naeem, F. Perveen, I.W. Khan, S. Saeed, J. Sahar, G. Abid, Utilization of indigenous gurgum (*Monotheca buxifolia*) waste seeds as a potential feedstock for biodiesel production using environmentally benign bismuth modified CaO catalyst, *Chem. Eng. Res. Des.* 183 (2022) 67–76, <https://doi.org/10.1016/j.cherd.2022.04.022>.
- [26] G. Fiorani, A. Perosa, M. Selva, Dimethyl carbonate: a versatile reagent for a sustainable valorization of renewables, *Green Chem.* 20 (2) (2018), <https://doi.org/10.1039/C7GC02118F>.
- [27] C. Gai, F. Zhang, Q. Lang, T. Liu, N. Peng, Z. Liu, Facile one-pot synthesis of iron nanoparticles immobilized into the porous hydrochar for catalytic decomposition of phenol, *Appl. Catal. B* 204 (2017) 566–576, <https://doi.org/10.1016/j.apcatb.2016.12.005>.

- [28] I. Ganesh, Conversion of carbon dioxide into methanol – a potential liquid fuel: fundamental challenges and opportunities (a review), *Renew. Sustain. Energy Rev.* 31 (2014) 221–257, <https://doi.org/10.1016/j.rser.2013.11.045>.
- [29] Y. Gao, C. Xu, Synthesis of dimethyl carbonate over waste eggshell catalyst, *Catal. Today* 190 (1) (2012) 107–111, <https://doi.org/10.1016/j.cattod.2011.12.004>.
- [30] P. Giannozzi, S. Baroni, N. Bonini, M. Calandra, R. Car, C. Cavazzoni, D. Ceresoli, G.L. Chiarotti, M. Cococcioni, I. Dabo, A. Dal Corso, S. de Gironcoli, S. Fabris, G. Fratesi, R. Gebauer, U. Gerstmann, C. Gougousis, A. Kokalj, M. Lazzeri, R. M. Wentzcovitch, QUANTUM ESPRESSO: a modular and open-source software project for quantum simulations of materials, *J. Phys. Condens. Matter* 21 (39) (2009), 395502, <https://doi.org/10.1088/0953-8984/21/39/395502>.
- [31] A.A. Greish, E.D. Finashina, O.P. Tkachenko, E.V. Shuvalova, L.M. Kustov, Synthesis of dimethyl carbonate from methanol and CO<sub>2</sub> on the SnO<sub>2</sub>/Al<sub>2</sub>O<sub>3</sub>-based catalyst, *Mendeleev Commun.* 26 (6) (2016), <https://doi.org/10.1016/j.mencom.2016.11.012>.
- [32] P. Hatefirad, M. Hosseini, A. Tavasoli, Effect of Fe/Cu catalysts supported on zeolite/active carbon hybrid on bio-oil quality derived from catalytic pyrolysis of granular bacteria biomass, *Fuel* 312 (2022), 122870, <https://doi.org/10.1016/j.fuel.2021.122870>.
- [33] M. Honda, S. Kuno, S. Sonehara, K. Fujimoto, K. Suzuki, Y. Nakagawa, K. Tomishige, Tandem carboxylation-hydration reaction system from methanol, CO<sub>2</sub> and benzonitrile to dimethyl carbonate and benzamide catalyzed by CeO<sub>2</sub>, *ChemCatChem* 3 (2) (2011) 365–370, <https://doi.org/10.1002/cctc.201000339>.
- [34] M. Honda, M. Tamura, Y. Nakagawa, S. Sonehara, K. Suzuki, K. Fujimoto, K. Tomishige, Ceria-catalyzed conversion of carbon dioxide into dimethyl carbonate with 2-cyanopyridine, *ChemSusChem* 6 (8) (2013), <https://doi.org/10.1002/cssc.201300229>.
- [35] IEA, Emissions Factors 2021, September, IEA, 2021. Emissions Factors 2021.
- [36] A. Jain, S.P. Ong, G. Hautier, W. Chen, W.D. Richards, S. Dacek, S. Cholia, D. Gunter, D. Skinner, G. Ceder, K.A. Persson, Commentary: the materials project: a materials genome approach to accelerating materials innovation, *APL Mater.* 1 (1) (2013), 011002, <https://doi.org/10.1063/1.4812323>.
- [37] S. Jain, A. Banswal, R.B. Biniwale, S. Milmille, S. Das, S. Tiwari, P. Siluvai Antony, Enhancing adsorption of nitrate using metal impregnated alumina, *J. Environ. Chem. Eng.* 3 (4) (2015) 2342–2349, <https://doi.org/10.1016/j.jece.2015.08.009>.
- [38] P.K. Jal, M. Sudarshan, A. Saha, S. Patel, B.K. Mishra, Synthesis and characterization of nanosilica prepared by precipitation method, *Colloids Surf. A* 240 (1–3) (2004) 173–178, <https://doi.org/10.1016/j.colsurfa.2004.03.021>.
- [39] I. Justo-Reinoso, M.T. Hernandez, C. Lucero, W.V. Srubar, Dispersion and effects of metal impregnated granular activated carbon particles on the hydration of antimicrobial mortars, *Cem. Concr. Compos.* 110 (2020), 103588, <https://doi.org/10.1016/j.cemconcomp.2020.103588>.
- [40] N. Keller, G. Rebmann, V. Keller, Catalysts, mechanisms and industrial processes for the dimethylcarbonate synthesis, *J. Mol. Catal. A Chem.* 317 (1–2) (2010) 1–18, <https://doi.org/10.1016/j.molcata.2009.10.027>.
- [41] Y. Kim, E. Cho, C.H. Ko, Preparation of Ni-based egg-shell-type catalyst on cylinder-shaped alumina pellets and its application for hydrogen production via steam methane reforming, *Int. J. Hydrogen Energy* 44 (11) (2019) 5314–5323, <https://doi.org/10.1016/j.ijhydene.2018.08.100>.
- [42] D. Klaus, F. Tilo, L. Thomas, in: T.S.R. Prasad Rao, G. Murali Dhar (Eds.), *Manufacturing of raw materials for the catalyst industry, Studies in Surface, Science and Catalysis* 113, Elsevier, 1998, pp. 599–611, [https://doi.org/10.1016/S0167-2991\(98\)80336-4](https://doi.org/10.1016/S0167-2991(98)80336-4). ISSN 0167-2991.
- [43] J.F. Knifton, R.G. Duranleau, Ethylene glycol—Dimethyl carbonate cogeneration, *J. Mol. Catal.* 67 (3) (1991) 389–399, [https://doi.org/10.1016/0304-5102\(91\)80051-4](https://doi.org/10.1016/0304-5102(91)80051-4).
- [44] T. Kulthananat, P. Kim-Lohsoontorn, P. Seeharaj, Ultrasonically assisted surface modified CeO<sub>2</sub> nanospindle catalysts for conversion of CO<sub>2</sub> and methanol to DMC, *Ultrason. Sonochem.* 90 (2022), 106164, <https://doi.org/10.1016/j.ultsonch.2022.106164>.
- [45] A. Laca, A. Laca, M. Diaz, Eggshell waste as catalyst: a review, *J. Environ. Manag.* 197 (2017) 351–359, <https://doi.org/10.1016/j.jenvman.2017.03.088>.
- [46] H.J. Lee, W. Joe, I.K. Song, Direct synthesis of dimethyl carbonate from methanol and carbon dioxide over transition metal oxide/CeO<sub>2</sub> catalysts: effect of acidity and basicity of the catalysts, *Korean J. Chem. Eng.* 29 (3) (2012), <https://doi.org/10.1007/s11814-011-0185-3>.
- [47] J.H. Lee, J.H. Kwon, J.W. Lee, H. Lee, J.H. Chang, B.I. Sang, Preparation of high purity silica originated from rice husks by chemically removing metallic impurities, *J. Ind. Eng. Chem.* 50 (2017), <https://doi.org/10.1016/j.jiec.2017.01.033>.
- [48] E. Leino, Transformation of Carbon Dioxide to Diethyl Carbonate over Ceria and Ceria-supported Catalysts, Finland (2015).
- [49] E. Leino, N. Kumar, P. Mäki-Arvela, A.R. Rautio, J. Dahl, J. Roine, J.P. Mikkola, Synthesis and characterization of ceria-supported catalysts for carbon dioxide transformation to diethyl carbonate, *Catal. Today* 306 (2018) 128–137, <https://doi.org/10.1016/j.cattod.2017.01.016>.
- [50] E. Leino, P. Mäki-Arvela, V. Eta, N. Kumar, F. Demoisson, A. Samikannu, A. R. Leino, A. Shchukarev, D.Y. Murzin, J.P. Mikkola, The influence of various synthesis methods on the catalytic activity of cerium oxide in one-pot synthesis of diethyl carbonate starting from CO<sub>2</sub>, ethanol and butylene oxide, *Catal. Today* 210 (2013) 47–54, <https://doi.org/10.1016/j.cattod.2013.02.011>.
- [51] H. Li, J. Zhao, R. Shi, P. Hao, S. Liu, Z. Li, J. Ren, Remarkable activity of nitrogen-doped hollow carbon spheres encapsulated Cu on synthesis of dimethyl carbonate: role of effective nitrogen, *Appl. Surf. Sci.* 436 (2018) 803–813, <https://doi.org/10.1016/j.apsusc.2017.12.092>.
- [52] Z. Li, K. Xie, R.C.T. Slade, High selective catalyst CuCl/MCM-41 for oxidative carbonylation of methanol to dimethyl carbonate, *Appl. Catal. A* 205 (1–2) (2001) 85–92, [https://doi.org/10.1016/S0926-860X\(00\)00546-9](https://doi.org/10.1016/S0926-860X(00)00546-9).
- [53] A.A. Marciniak, O.C. Alves, L.G. Appel, C.J.A. Mota, Synthesis of dimethyl carbonate from CO<sub>2</sub> and methanol over CeO<sub>2</sub>: role of copper as dopant and the use of methyl trichloroacetate as dehydrating agent, *J. Catal.* 371 (2019), <https://doi.org/10.1016/j.jcat.2019.01.035>.
- [54] A.A. Marciniak, F.J.F.S. Henrique, A.F.F. de Lima, O.C. Alves, C.R. Moreira, L. G. Appel, C.J.A. Mota, What are the preferred CeO<sub>2</sub> exposed planes for the synthesis of dimethyl carbonate? answers from theory and experiments, *Mol. Catal.* 493 (2020), <https://doi.org/10.1016/j.mcat.2020.111053>.
- [55] F. Mariño, I. Iglesias, G. Baronetti, L. Alemany, M. Laborde, Egg-shell CuO/CeO<sub>2</sub>/Al<sub>2</sub>O<sub>3</sub> catalysts for CO preferential oxidation, *Int. J. Hydrogen Energy* 40 (34) (2015) 11235–11241, <https://doi.org/10.1016/j.ijhydene.2015.03.051>.
- [56] M. Mariyaselvakumar, T. Selvaraj, V. Balasubramanian, K. Srinivasan, Direct synthesis of dimethyl carbonate from methanol and carbon dioxide over nickel loaded ceria as improved catalysts, *React. Kinet. Mech. Catal.* 135 (2) (2022) 937–950, <https://doi.org/10.1007/s11444-022-01262-5>.
- [57] N. Massoni, R.J. Koch, A. Hertz, L. Campayo, M.P. Moloney, S.T. Misture, A. Grandjean, Structural effects of calcination on Cs-exchanged copper hexacyanoferrate (Cs<sub>2</sub>K<sub>2</sub>CuFe(CN)<sub>6</sub>) loaded on mesoporous silica particles, *J. Nucl. Mater.* 528 (2020), 151887, <https://doi.org/10.1016/j.jnucmat.2019.151887>.
- [58] J.D. Medrano-García, J. Javaloyes-Antón, D. Vázquez, R. Ruiz-Femenia, J. A. Caballero, Alternative carbon dioxide utilization in dimethyl carbonate synthesis and comparison with current technologies, *J. CO<sub>2</sub> Util.* 45 (2021), 101436, <https://doi.org/10.1016/j.jcou.2021.101436>.
- [59] F.J. Méndez, J.A. Alves, Y. Rojas-Challa, O. Corona, Y. Villasana, J. Guerra, G. García-Colli, O.M. Martínez, J.L. Brito, An egg-shell bifunctional CeO<sub>2</sub>-modified NiPd/Al<sub>2</sub>O<sub>3</sub> catalyst for petrochemical processes involving selective hydrogenation and hydroisomerization, *J. Rare Earths* 39 (11) (2021) 1382–1388, <https://doi.org/10.1016/j.jre.2020.09.017>.
- [60] N. Miralles, J.E. Gómez, A.W. Kleij, E. Fernández, Copper-mediated S N<sup>2</sup> Allyl-Alkyl and allyl-boryl couplings of vinyl cyclic carbonates, *Org. Lett.* 19 (22) (2017) 6096–6099, <https://doi.org/10.1021/acs.orglett.7b02947>.
- [61] A. Mullick, S. Neogi, Ultrasound assisted synthesis of Mg-Mn-Zr impregnated activated carbon for effective fluoride adsorption from water, *Ultrason. Sonochem.* 50 (2019) 126–137, <https://doi.org/10.1016/j.ultsonch.2018.09.010>.
- [62] C.G. Okoye-Chine, C.O.L. Mbuya, T.S. Ntelane, M. Moyo, D. Hildebrandt, The effect of silanol groups on the metal-support interactions in silica-supported cobalt Fischer-Tropsch catalysts: a temperature programmed surface reaction, *J. Catal.* 381 (2020) 121–129, <https://doi.org/10.1016/j.jcat.2019.10.036>.
- [63] P. Oulego, A. Laca, S. Calvo, M. Díaz, Eggshell-supported catalysts for the advanced oxidation treatment of humic acid polluted wastewaters, *Water* 12 (1) (2019) 100, <https://doi.org/10.3390/w12010100> (Basel).
- [64] W. Peng, N. Zhao, F. Xiao, W. Wei, Y. Sun, Recent progress in phosgene-free methods for synthesis of dimethyl carbonate, *Pure Appl. Chem.* 84 (3) (2011) 603–620, <https://doi.org/10.1351/PAC-CON-11-06-02>.
- [65] J.P. Perdew, K. Burke, M. Ernzerhof, Generalized gradient approximation made simple, *Phys. Rev. Lett.* 77 (18) (1996) 3865–3868, <https://doi.org/10.1103/PhysRevLett.77.3865>.
- [66] G. Pradhan, Y.C. Sharma, Green synthesis of glycerol carbonate by transesterification of bio glycerol with dimethyl carbonate over Mg/ZnO: a highly efficient heterogeneous catalyst, *Fuel* 284 (2021), <https://doi.org/10.1016/j.fuel.2020.118966>.
- [67] W. Praikaew, W. Kiattkitipong, F. Aiouache, Y. Najdanovic-Visak, M. Termtanun, J.W. Lim, S.S. Lam, K. Kiattkitipong, N. Laosiripojana, S. Boonyasuwat, S. Assabumrungrat, Mechanism of  $\text{CaO}/\text{CaO}$ -catalyst deactivation with unconventional monitoring method for glycerol carbonate production via transesterification of glycerol with dimethyl carbonate, *Int. J. Energy Res.* 46 (2) (2022) 1646–1658, <https://doi.org/10.1002/er.7281>.
- [68] B. Qiao, T.J. Wang, H. Gao, Y. Jin, High density silanization of nano-silica particles using  $\gamma$ -aminopropyltriethoxysilane (APTES), *Appl. Surf. Sci.* 351 (2015) 646–654, <https://doi.org/10.1016/j.apsusc.2015.05.174>.
- [69] W.U. Rahman, A. Fatima, A.H. Anwer, M. Athar, M.Z. Khan, N.A. Khan, G. Halder, Biodiesel synthesis from eucalyptus oil by utilizing waste egg shell derived calcium based metal oxide catalyst, *Process Saf. Environ. Prot.* 122 (2019) 313–319, <https://doi.org/10.1016/j.psep.2018.12.015>.
- [70] T. Risthaus, S. Grimme, Benchmarking of London dispersion-accounting density functional theory methods on very large molecular complexes, *J. Chem. Theory Comput.* 9 (3) (2013) 1580–1591, <https://doi.org/10.1021/ct301081n>.
- [71] D.M. Rodrigues, L.M. dos Santos, F.L. Bernard, I.S. Pinto, R. Zampiva, G. Kaufmann, S. Einloft, Imidazolium-based ionic liquid silica xerogel as catalyst to transform CO<sub>2</sub> into cyclic carbonate, *SN Appl. Sci.* 2 (12) (2020) 1936, <https://doi.org/10.1007/s42452-020-03712-z>.
- [72] D.M. Rodrigues, L.M. dos Santos, F.L. Bernard, I.S. Pinto, R. Zampiva, G. Kaufmann, S. Einloft, Imidazolium-based ionic liquid silica xerogel as catalyst to transform CO<sub>2</sub> into cyclic carbonate, *SN Appl. Sci.* 2 (12) (2020) 1936, <https://doi.org/10.1007/s42452-020-03712-z>.
- [73] S.A. Aquino, O.M. Vieira, A.S.D. Ferreira, E.J. Cabrita, S. Einloft, O.M. de Souza, Hybrid ionic liquid-silica xerogels applied in CO<sub>2</sub> capture, *Appl. Sci.* 9 (13) (2019), <https://doi.org/10.3390/app9132614>.
- [74] R. Saada, S. Kellici, T. Heil, D. Morgan, B. Saha, Greener synthesis of dimethyl carbonate using a novel ceria-zirconia oxide/graphene nanocomposite catalyst, *Appl. Catal. B* 168–169 (2015) 353–362, <https://doi.org/10.1016/j.apcatb.2014.12.013>.

- [75] T. Sakakura, J.C. Choi, H. Yasuda, Transformation of carbon dioxide, *Chem. Rev.* 107 (6) (2007) 2365–2387, <https://doi.org/10.1021/cr068357u>.
- [76] A. Sánchez, L.M. Gil, M. Martín, Sustainable DMC production from CO<sub>2</sub> and renewable ammonia and methanol, *J. CO<sub>2</sub> Util.* 33 (2019) 521–531, <https://doi.org/10.1016/j.jcou.2019.08.010>.
- [77] J.A. Santana Costa, C.M. Paranhos, Systematic evaluation of amorphous silica production from rice husk ashes, *J. Clean. Prod.* 192 (2018), <https://doi.org/10.1016/j.jclepro.2018.05.028>.
- [78] B. Schäffner, F. Schäffner, S.P. Verevkin, A. Börner, Organic carbonates as solvents in synthesis and catalysis, *Chem. Rev.* 110 (8) (2010) 4554–4581, <https://doi.org/10.1021/cr900393d>.
- [79] Y. Shen, P. Zhao, Q. Shao, Porous silica and carbon derived materials from rice husk pyrolysis char, *Microporous Mesoporous Mater.* 188 (2014), <https://doi.org/10.1016/j.micromeso.2014.01.005>.
- [80] H. Sun, H. Li, X. Chang, S. Miao, X. Yuan, W. Zhang, M. Jia, Nitrogen-doped carbon supported ZnO as highly stable heterogeneous catalysts for transesterification synthesis of ethyl methyl carbonate, *J. Colloid Interface Sci.* 581 (2021) 126–134, <https://doi.org/10.1016/j.jcis.2020.07.095>.
- [81] W. Sun, L. Zheng, Y. Wang, D. Li, Z. Liu, L. Wu, T. Fang, J. Wu, Study of thermodynamics and experiment on direct synthesis of dimethyl carbonate from carbon dioxide and methanol over yttrium oxide, *Ind. Eng. Chem. Res.* 59 (10) (2020) 4281–4290, <https://doi.org/10.1021/acs.iecr.9b06092>.
- [82] Z.G.K.D. Szabó, Contact catalysis. Contributions by the Members of the Catalysis Club of Te Hungarian Academy of Sciences, Akadémiai Kiadó, Budapest, 1976.
- [83] K. Tomishige, Y. Ikeda, T. Sakaihari, K. Fujimoto, Catalytic properties and structure of zirconia catalysts for direct synthesis of dimethyl carbonate from methanol and carbon dioxide, *J. Catal.* 192 (2) (2000), <https://doi.org/10.1006/jcat.2000.2854>.
- [84] K. Tomishige, T. Sakaihari, Y. Ikeda, K. Fujimoto, A novel method of direct synthesis of dimethyl carbonate from methanol and carbon dioxide catalyzed by zirconia, *Catal. Lett.* 58 (4) (1999), <https://doi.org/10.1023/A:1019098405444>.
- [85] H.H. Tseng, M.Y. Wey, C.H. Fu, Carbon materials as catalyst supports for SO<sub>2</sub> oxidation: catalytic activity of CuO–AC, *Carbon N Y* 41 (1) (2003) 139–149, [https://doi.org/10.1016/S0008-6223\(02\)00264-6](https://doi.org/10.1016/S0008-6223(02)00264-6).
- [86] T. Tsoncheva, I. Genova, D. Paneva, M. Dimitrov, B. Tsyntarski, N. Velinov, R. Ivanova, G. Issa, D. Kovacheva, T. Budinova, I. Mitov, N. Petrov, Cobalt- and iron-based nanoparticles hosted in SBA-15 mesoporous silica and activated carbon from biomass: effect of modification procedure, *Solid State Sci.* 48 (2015) 286–293, <https://doi.org/10.1016/j.solidstatesciences.2015.09.001>.
- [87] K. Vinayakumar, A. Palliyarayil, P. Seethur Prakash, S. Nandakumar, N. Shunmuga Kumar, S. Sil, Studies on the deactivation and activation of palladium impregnated carbon catalyst for environmental applications, *Mater. Today: Proc.* 31 (2020) 631–639, <https://doi.org/10.1016/j.matpr.2020.05.110>.
- [88] S. Wada, K. Oka, K. Watanabe, Y. Izumi, Catalytic conversion of carbon dioxide into dimethyl carbonate using reduced copper-cerium oxide catalysts as low as 353 K and 1.3 MPa and the reaction mechanism, *Front. Chem.* 1 (2013), <https://doi.org/10.3389/fchem.2013.00008>.
- [89] S. Wang, J. Zhou, S. Zhao, Y. Zhao, X. Ma, Enhancement of dimethyl carbonate synthesis with *in situ* hydrolysis of 2,2-dimethoxy propane, *Chem. Eng. Technol.* 39 (4) (2016) 723–729, <https://doi.org/10.1002/ceat.201400603>.
- [90] S.P. Wang, J.J. Zhou, S.Y. Zhao, Y.J. Zhao, X.B. Ma, Enhancements of dimethyl carbonate synthesis from methanol and carbon dioxide: the *in situ* hydrolysis of 2-cyanopyridine and crystal face effect of ceria, *Chin. Chem. Lett.* 26 (9) (2015), <https://doi.org/10.1016/j.ccl.2015.05.005>.
- [91] J. Xu, N. Gao, D. Zhao, Z. Liu, M. Tang, Y. Chen, Y. Zhu, Different iron salt impregnated granular activated carbon (Fe-GAC) for perchlorate removal: characterization, performance and mechanism, *Colloids Surf. A* 509 (2016) 99–108, <https://doi.org/10.1016/j.colsurfa.2016.08.039>.
- [92] Z. Xu, J. Wang, J. Yang, X. Miao, R. Chen, J. Qian, R. Miao, Enhanced performance of a lithium-sulfur battery using a carbonate-based electrolyte, *Angew. Chem. Int. Ed.* 55 (35) (2016) 10372–10375, <https://doi.org/10.1002/anie.201605931>.
- [93] K. Xuan, S. Chen, Y. Pu, Y. Guo, Y. Guo, Y. Li, C. Pu, N. Zhao, F. Xiao, Encapsulating phosphotungstic acid within metal-organic framework for direct synthesis of dimethyl carbonate from CO<sub>2</sub> and methanol, *J. CO<sub>2</sub> Util.* 59 (2022), 101960, <https://doi.org/10.1016/j.jcou.2022.101960>.
- [94] K. Xuan, Y. Pu, F. Li, J. Luo, N. Zhao, F. Xiao, Metal-organic frameworks MOF-808-X as highly efficient catalysts for direct synthesis of dimethyl carbonate from CO<sub>2</sub> and methanol, *Chin. J. Catal.* 40 (4) (2019) 553–566, [https://doi.org/10.1016/S1872-2067\(19\)63291-2](https://doi.org/10.1016/S1872-2067(19)63291-2).
- [95] G. Yang, A. Jia, J. Li, F. Li, Y. Wang, Investigation of synthesis parameters to fabricate CeO<sub>2</sub> with a large surface and high oxygen vacancies for dramatically enhanced performance of direct DMC synthesis from CO<sub>2</sub> and methanol, *Mol. Catal.* 528 (2022), 112471, <https://doi.org/10.1016/j.mcat.2022.112471>.
- [96] P. Yang, Y. Cao, W.L. Dai, J.F. Deng, K.N. Fan, Effect of chemical treatment of activated carbon as a support for promoted dimethyl carbonate synthesis by vapor phase oxidative carbonylation of methanol over Wacker-type catalysts, *Appl. Catal. A* 243 (2) (2003) 323–331, [https://doi.org/10.1016/S0926-860X\(02\)00567-7](https://doi.org/10.1016/S0926-860X(02)00567-7).
- [97] Y. Wang, Z. Liu, C. Tan, H. Sun, Z. Li, The influence of iron group promoters on the synthesis of dimethyl carbonate over CuY catalysts prepared via modified vapor impregnation method, *Russ. J. Phys. Chem. A* 95 (4) (2021) 705–712, <https://doi.org/10.1134/S0036024421040269>.
- [98] A.S. Yusuff, A.O. Gbadamosi, N. Atray, Development of a zeolite supported CaO derived from chicken eggshell as active base catalyst for used cooking oil biodiesel production, *Renew. Energy* 197 (2022) 1151–1162, <https://doi.org/10.1016/j.renene.2022.08.032>.
- [99] M. Zhang, Y. Xu, B.L. Williams, M. Xiao, S. Wang, D. Han, L. Sun, Y. Meng, Catalytic materials for direct synthesis of dimethyl carbonate (DMC) from CO<sub>2</sub>, *J. Clean. Prod.* 279 (2021), 123344, <https://doi.org/10.1016/j.jclepro.2020.123344>.
- [100] Z.F. Zhang, Z.T. Liu, Z.W. Liu, J. Lu, DMC formation over Ce<sub>0.5</sub>Zr<sub>0.5</sub>O<sub>2</sub> prepared by complex-decomposition method, *Catal. Lett.* 129 (3–4) (2009) 428–436, <https://doi.org/10.1007/s10562-008-9816-7>.
- [101] Q. Zheng, R. Nishimura, Y. Sato, H. Inomata, M. Ota, M. Watanabe, S. Camy, Dimethyl carbonate (DMC) synthesis from methanol and carbon dioxide in the presence of ZrO<sub>2</sub> solid solutions and yield improvement by applying a natural convection circulation system, *Chem. Eng. J.* 429 (2022), 132378, <https://doi.org/10.1016/j.cej.2021.132378>.